The northern European shelf as increasing net sink for CO_2

Meike Becker[1,2], Are Olsen[1,2], Peter Landschützer[3], Abdirhaman Omar[4,2], Gregor Rehder[5], Christian Rödenbeck[6], and Ingunn Skjelvan[4,2]

[1]Geophysical Institute, University of Bergen, Bergen, Norway
[2]Bjerknes Center for Climate Research, Bergen, Norway
[3]Max Planck Institute for Meteorology, Hamburg, Germany
[4]NORCE Norwegian Research Centre AS, Bergen, Norway
[5]Leibniz Institute for Baltic Sea Reasearch, Warnemünde, Germany
[6]Max Planck Institute for Biogeochemistry, Jena, Germany

Correspondence: Meike Becker (meike.becker@uib.no)

Abstract. We developed a simple method to refine existing open ocean maps and extending them towards different coastal seas. Using a multi linear regression we produced monthly maps of surface ocean $f\mathrm{CO_2}$ in the northern European coastal seas (North Sea, Baltic Sea, Norwegian Coast and in the Barents Sea) covering a time period from 1998 to 2016. A comparison with gridded SOCAT v5 data revealed standard deviations and residuals of $0\pm26\mu$atm in the North Sea, $0\pm16\mu$atm along the Norwegian Coast, $0\pm19\mu$atm in the Barents Sea, and $2\pm42\mu$atm in the Baltic Sea. We used these maps as basis to investigate trends in $f\mathrm{CO_2}$, pH and air-sea CO_2 flux. The surface ocean $f\mathrm{CO_2}$ trends are smaller than the atmospheric trend in most of the studied regions. Only in the western part of the North Sea we found an increase in $f\mathrm{CO_2}$ close to 2 μatm yr^{-1}, which is similar to the atmospheric trend. The Baltic Sea does not show a significant trend. Here, the variability was much larger than the expected trends. Consistently, the pH trends were smaller than expected for an increase of $f\mathrm{CO_2}$ in pace with the rise of atmospheric CO_2 levels. The calculated air-sea CO_2 fluxes revealed that most regions were net sinks for CO_2. Only the southern North Sea and the Baltic Sea emitted CO_2 to the atmosphere. Especially in the northern regions the sink strength increased during the studied period.

1 Introduction

For facing global challenges, such as predicting and tracking climate change, it is important to improve our understanding of the ocean carbon sink and its variability. Open oceans, especially those of the northern hemisphere, are relatively well understood and described in their large-scale variability (Gruber et al., 2019; Landschützer et al., 2018, 2019; Fay and McKinley, 2017). Reliable autonomous systems for measuring carbon dioxide partial pressure from commercial vessels were developed in the early 2000s (Pierrot et al., 2009) and have since been deployed on a large number of vessels (e.g. (Bakker et al., 2016)). This has resulted in sufficient data to develop methods to interpolate the data and to describe large scale air-sea CO_2 exchange and its

variability (Landschützer et al., 2014, 2013; Rödenbeck et al., 2013; Jones et al., 2015). These methods cover a wide variety of approaches, such as linear interpolations, machine learning, and model based estimates. By comparing the different results it is possible to achieve a good estimate of the uncertainty associated with the respective methods and to evaluate their performance relative to each other (Rödenbeck et al., 2015).

5   Despite coastal seas cover 7-10% of the world's oceans (Bourgeois et al., 2016), their contribution to the oceanic carbon sink is not yet fully constrained. Whether coastal seas are a net sink or source for atmospheric CO_2 and how their role will change in a changing climate is still under debate (Bauer et al., 2013; Laruelle et al., 2010). Compared to the open ocean, longer time series and a higher spatial and temporal resolution of the observations are needed in order to capture all relevant coastal processes. Small scale circulation patterns governed by topographic features, thermal and haline stratification, or mixing 10 through tidal cycles, upwelling or internal waves result in a need for more complex maps with a higher resolution (Bricheno et al., 2014; Lima and Wethey, 2012; Blanton, 1991). These physical drivers are not the only reasons for coastal seas being more complicated to understand. Generally, coastal regions show a larger productivity than open ocean regions due to different additional sources of nutrients (e.g. mixing at continental margins, river runoff). While deeper regions are seasonally stratified, shallow regions are vertically mixed allowing for exchange between the benthic and pelagic parts of the ecosystem (Griffiths 15 et al., 2017; Wollast, 1998). Together with strong gradients of productivity this leads to spatial and temporal heterogeneity in surface CO_2 content.

    The different maps developed for describing the open ocean surface pCO_2 (CO_2 partial pressure) dynamics and air-sea CO_2 fluxes are not directly suitable for the application in coastal regions. Many exclude data from continental shelves completely while all of them have a too coarse spatial resolution (typically between 1 and 5 $^\circ$) to properly resolve coastal seas with 20 their small-scale variability. A few studies tried to describe coastal carbon dynamics but most of them have strong regional or temporal limitations. Table 1 shows an overview of studies with estimated pCO_2 trends over the northern European shelf while Table 2 presents available flux estimates. Laruelle et al. (2017) used a neural network approach to produce a global pCO_2 climatology of coastal seas, describing more distinct seasonal variability in the northern hemisphere than in the southern Pacific and Atlantic. Few studies attempted to constrain coastal air-sea fluxes before. Laruelle et al. (2018) published trend estimates 25 in regions with high data coverage based on winter data spanning up to 35 years. They find the pCO_2 rise in coastal regions to lag behind the atmospheric rise in CO_2. For the Baltic Sea, Parard et al. (2016, 2017) used a neural network approach to produce surface ocean pCO_2 maps from 1998 to 2011 and estimated an air-sea flux of 1.2 mmol m^{-2} day^{-1}. Yasunaka et al. (2018) estimated a flux of 8 - 12 mmol m^{-2} day^{-1} in the Barents Sea and along the Norwegian coast using a self-organizing map technique. Most of the other available studies on the trends in coastal pCO_2 are based on data from either summer or 30 winter. Estimates based on summer-only data typically show large interannual variations (Thomas et al., 2007; Salt et al., 2013), which led to the conclusion that here the interannual variability masks the actual long term trend. The approach to use winter-only data (Fröb et al., 2019; Omar et al., 2019), on the other hand, is based on the assumption that during this season the influence of biological processes is negligible and therefore winter data can be used to establish a baseline trend. However, also using winter-only data has its drawbacks. In particular the choice of which months to include can cause biases and the 35 optimal selection can differ from region to region .

Table 1. Overview of trends in surface ocean CO_2 reported in the literature.

	Reference	Time range	$dpCO_2/dt$ /μatm yr^{-1}
North Sea	Thomas et al. (2007)	2001-2005, summer data normalized to 16°	7.9
North Sea	Salt et al. (2013)	2001-2005, summer data, normalized to 16°	6.5
North Sea	Salt et al. (2013)	2005-2008, summer data, normalized to 16°	1.33
Faeroe Banks	Fröb et al. (2019)	2004-2017, winter data (DJFM)	2.25 ± 0.20
North Sea, west	Omar et al. (2019)	2004-2017, winter data (DJ)	2.19 ± 0.55
North Sea, east	Omar et al. (2019)	2004-2017, winter data (DJF)	not significant
North Sea	Laruelle et al. (2018)	1988-2015	almost no trend
English channel	Laruelle et al. (2018)	1988-2015	slightly smaller than atmosphere
Baltic Sea	Wesslander et al. (2010)	1994-2008	larger than atmosphere
Baltic Sea	Schneider and Müller (2018)	2008-2015	4.6 - 6.1
Baltic Sea, west	Laruelle et al. (2018)	1988-2015	much smaller than atmosphere, slightly negative
Barents Sea	Yasunaka et al. (2018)	1997-2013	not significant
Barents Sea	Laruelle et al. (2018)	1988-2015	about the same as atmosphere
Atmosphere	global average	1997-2016	2.02 ppm yr^{-1}

Table 2. Overview of air-sea CO_2 fluxes reported in the literature. Negative sign denotes flux from atmosphere to ocean.

	Reference	Time range	F / mmol m^{-2} day^{-1}
North Sea	Meyer et al. (2018)	2001/2002	-3.8
Baltic Sea	Parard et al. (2017)	1998-2011	1.2
Norwegian Coast	Yasunaka et al. (2018)	1997-2013	-4 - -8
Barents Sea	Yasunaka et al. (2018)	1997-2013	-8 - -12

In this study we present a new approach to develop monthly $f\text{CO}_2$ (CO_2 fugacity) maps based on already existing open ocean $p\text{CO}_2$ maps, in four example regions: North Sea, Baltic Sea, Norwegian Coast and the Barents Sea. A multi linear regression (MLR) was used to fit driver data against $f\text{CO}_2$ observations. Based on the resulting $f\text{CO}_2$ maps and a salinity-alkalinity correlation we also produced monthly maps of coastal pH. The performance of the produced maps was evaluated and the maps were then used to investigate trends in coastal $f\text{CO}_2$ and pH in the entire region from 1998 to 2016. Finally, we used the $f\text{CO}_2$ maps to determine the air-sea CO_2 exchange and show its temporal and spatial patterns. ß

2 Method

2.1 Study area

This work focuses on the northern European continental shelf and marginal seas. As we want to show the performance of the MLR method we picked a number of regions with very different characteristics: the North Sea, the Baltic Sea, the Norwegian coast and the western Barents Sea (Figure 1). We decided to concentrate on these regions because (1) the data coverage in these regions is fairly high and (2) the authors have strong knowledge on the specific regions. This is important in order to properly evaluate the maps and to assess whether or not the output is realistic. The four regions were defined based on the COastal Segmentation and related CATchments (COSCAT) segmentation scheme (Laruelle et al., 2013). The threshold for defining a region as coastal sea was set to a depth limit of 500 m. By using this definition, we produce an overlap to the open ocean maps, allowing our maps to be merged with the open ocean maps. Please note, that this study concentrates on the continental shelf area. the near coastal zones (e.g. intertidal zones) are not included due to the limited availability of driver data in these regions.

2.2 Data handling

The CO_2 data used in this study were extracted from SOCAT version 5 (Bakker et al., 2016). Their coverage is shown in Figure 2. A newer version of the SOCAT database (SOCATv2019) was used for validating the maps against independent data. An overview over the reanalysis products used as driver data is given in Table 3. We use as basic driver data sea surface temperature (SST), sea surface salinity (SSS), chlorophyll a concentration (Chl a), mixed layer depth (MLD), bathymetry (BAT), distance from shore (DIST), ice concentration (ICE), the change in ice concentration from month to month. Chl a values during the dark winter season were set to 0. In addition to the reanalysis data, $p\text{CO}_2$ values from the closest coastal grid cell of the open ocean map were used as a driver in our MLR. We can neglect the difference between partial pressure and fugacity of CO_2 (about 1 μatm) at this place as it is much smaller than the accuracy of the data extracted from SOCAT v5 (2 to 10 μatm) and the uncertainty associated to the open ocean maps. The open ocean $p\text{CO}_2$ values were extracted from two different products (Rödenbeck et al. (2014) (version oc_v1.5) and Landschützer et al. (2017, 2016) (version 2016)). Rödenbeck et al. (2014) is based on a data-driven diagnostic model of ocean biogeochemistry fitted against surface $p\text{CO}_2$ observations while Landschützer et al. (2016) uses a two-step neural network (a feed-forward network coupled with self-organizing maps, FFN-SOM) trained with the $p\text{CO}_2$ observations. Please note that the Rödenbeck open ocean map also contains data in coastal grid boxes, while

Table 3. Products used as driver data in the MLR and the maps.

Product used	Resolution	Reference
Chl a for MLR	4km x 4km, 8 days	Global Ocean Chlorophyll (Copernicus-GlobColour)
		from Satellite Observations - Reprocessed
Chl a for maps	4km x 4km, monthly	Global Ocean Chlorophyll (Copernicus-GlobColour)
		from Satellite Observations - Reprocessed
MLD	12.5km x 12.5km, monthly	Arctic Ocean Physics Reanalysis
ICE	0.25°x0.25°, monthly	Cavalieri et al. (1996)
SST / SSS	0.25°x0.25°, weekly	Global Ocean Observation-based Products
		Global_Rep_Phy_001_021
BAT	2min x 2min	ETOPO2v2 Center (2006)
Rödenbeck pCO_2	5° x 4°, monthly	Rödenbeck et al. (2014)
Landschützer pCO_2	1° x 1°, monthly	Landschützer et al. (2017)

the Landschützer open ocean map is restricted to the open ocean regions south of 80°N. The MLR models based on these two are called MLR 1 (based on the coastal pCO_2 values from the Rödenbeck map) and MLR 2 (based on the the nearest open ocean pCO_2 values of the Landschützer map), respectively. To determine the extent to which the regressions benefit from the information in the open ocean maps, a third MLR, MLR 3, was determined. Here, we do not use any of the open ocean maps

5   as driver, but instead the year as a proxy for the annual rise in CO_2.

For producing the input data for the MLR, each SOCAT $f CO_2$ data point was assigned to the closest data point in space and time of each of the reanalysis data. This produces a matrix as long as the SOCAT $f CO_2$ observations for each driver data. After this, the $f CO_2$ data as well as all driver data were binned on a monthly 0.125°x0.125° grid covering 1998 to 2016. This step ensures that the driver data have the same bias in space and time within each grid box as the $f CO_2$ data. If a grid box for

10   example only contains observations from the first week of the month and the northwestern corner, we make sure, that also the gridded driver data only contains values from the first week and the northwestern corner of the grid box, and not an average over the entire month and grid box. This is mostly important for the chlorophyll driver data, which are available in a very high resolution compared to the $f CO_2$ maps produced in this work. These driver data were used for the MLR.

For producing the final maps, a second set of the driver data was produced, in the following called field data. Here the

15   driver data were directly regridded to a monthly 0.125°x0.125° grid, providing the full spatial and temporal coverage and a homogeneous average in each grid box. The field data were used to produce the $f CO_2$ maps based on the equation derived from the MLR.

2.3   Multi linear regression

The multi linear regression models were constructed by forward and backward stepwise regression using the driver data as

20   predictor variables to model the $f CO_2$ observations. During a stepwise regression in each step, a variable is tested for being
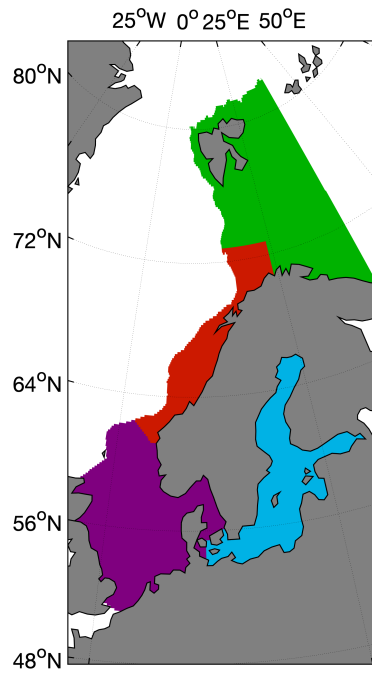
Figure 1. The study area and the location of the four different regions North Sea (purple), Norwegian Coast (red), Barents Sea (green) and Baltic Sea (blue).
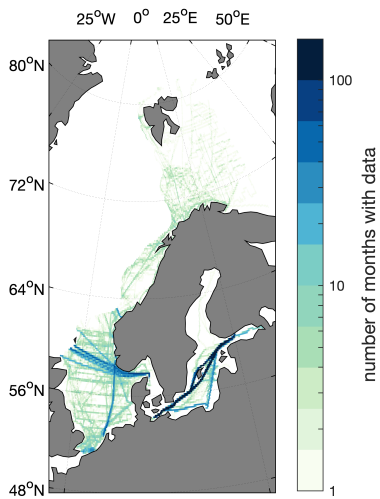
Figure 2. The number of months with $f\mathrm{CO_2}$ data from SOCAT v5 in each grid box.

Table 4. Driver used in the different regressions.

	MLD	SST	SSS	CHL	ICE	ICE change	BAT	DIST	$p\mathrm{CO_2}$	year
North Sea										
MLR 1	x	x	x	x	x		x		x	
MLR 2	x	x	x	x	x	x	x	x	x	
MLR 3	x	x	x	x	x	x	x	x		x
Norwegian Coast										
MLR 1	x	x	x	x	x		x		x	
MLR 2	x	x	x	x	x	x	x		x	
MLR 3	x	x	x	x	x	x	x			x
Barents Sea										
MLR 1	x	x	x	x	x	x	x		x	
MLR 2	x	x	x	x	x	x	x		x	
MLR 3	x	x	x	x	x	x	x			x
Baltic Sea										
MLR 1	x	x	x	x	x	x	x		x	
MLR 2	x	x	x	x	x	x	x		x	
MLR 3	x	x	x	x	x		x			x

added or removed from the set of explanatory variables. This decision on whether to add or remove a term was based on the p-value of the F-statistic with or without the term in question. The entrance tolerance was set to 0.05 and the exit tolerance to 0.1. The model includes constant, linear, and quadratic terms as well as products of linear terms. Equation 1 gives the basic equation, with $X_1...X_n$ being the driver data and $a_1...a_{nn}$ the regression coefficients.

$$y = a_0 + a_1 \cdot X_1 + ... + a_n \cdot X_n + a_{12} \cdot X_1 X_2 + ... + a_{mn} \cdot X_m X_n + a_{11} \cdot X_1^2 + ... + a_{nn} \cdot X_n^2 \tag{1}$$

The $p\mathrm{CO_2}$ value of the respective open ocean maps (MLR 1 and MLR 2), or the year were added (MLR 3). Inclusion of stationary drivers (such as month, latitude and longitude) in the MLR increased the performance of MLR 2 and MLR 3. However, these were still not better than MLR 1 and we therefore decided to limit this analysis to dynamic parameters. Using dynamic drivers only assures a dynamic description of the conditions in the field, and gives us the possibility to reproduce changes caused by a regime shifts, for example the ongoing atlantification of the Barents Sea (Oziel et al., 2016; Lind et al., 2018).

2.4 Validation

The three linear fits were compared to each other by taking into account the R^2 and the root mean square error (RMSE) of the fit, and the Nash Sutcliffe method efficiency (ME) (Nondal et al., 2009). The method efficiency compares how well the

model output (E_n) fits the observations (I_n) for every data point n to how well a simple monthly average ($\overline{I}$) would fit the observations:

$$\text{ME} = \frac{\sum_n \left(I_n - E_n\right)^2}{\sum_n \left(I_n - \overline{I}\right)^2} \tag{2}$$

A method efficiency >1 means that using just monthly averages of all data in the region would fit better to measured data than the respective model, Generally, a method efficiency >0.8 is considered bad. Besides the statistics of the fit itself, the final maps were also compared to the gridded SOCAT v5 data, resulting in an average offset and standard deviation. In order to compare the maps against data that were not used to produce the maps, we predicted the $f\text{CO}_2$ for the years 2017 and 2018 (ie, we applied the trained multi-linear model to driver data from 2017 and 2018) and compared these maps to $f\text{CO}_2$ observations in SOCAT v2019, gridded on a monthly $0.125°\text{x}0.125°$ grid. We also compare the maps directly with observations from time series in the North Sea and the Baltic Sea.

2.5 Ocean acidification

For calculating the pH, alkalinity (AT) was estimated in the North Sea, along the Norwegian Coast, and in the Barents Sea via a salinity-alkalinity correlation after Nondal et al. (2009). Alkalinity describes the capacity of the sea water to buffer changes in pH. As the concentration of most of the weak acids in seawater is strongly dependent on the salinity, alkalinity can in many regions be estimated from salinity. However, in regions with a high amount of organic acids in seawater, for example in strong blooms or at river mouths, deviations from the alkalinity-salinity relationship can be observed. The carbonate system was calculated using the CO2SYS program (van Heuven et al., 2009) with carbonic acid dissociation constants of Mehrbach et al. (1973) as refitted by Dickson and Millero (1987), KSO_4^- dissociation constants after Dickson (1990) and the boron-salinity relation after Uppström (1974). For the Baltic Sea, we did not calculate pH as the alkalinity-salinity relationship in this region is complex due to different AT-S relations in different sub-regions of the Baltic Sea, and a non-negligible increase of AT over the last 25 years (Müller et al., 2016).

2.6 Calculation of trends

For calculating trends of $f\text{CO}_2$ and ocean acidification, the data in every grid box were deseasonalised by subtracting the long-term averages of the respective months. Then a linear fit was applied to the deseasonalised time-series. For illustrating the influence of interannual variability we calculated the trend for different time ranges. As a time range less than 10 years barely resulted in significant trends, we decided to limit the trend analysis to starting years from 1998 to 2006 and ending years from 2008 to 2016.

2.7 Flux calculation

The air-sea disequilibrium was calculated as the difference between our mapped $f\text{CO}_2$ values and atmospheric $f\text{CO}_2$ in each grid cell and time step. The atmospheric $f\text{CO}_2$ was determined by converting the $x\text{CO}_2$ from the NOAA Marine Boundary

Layer Reference product from the NOAA GMD Carbon Cycle Group into $f\mathrm{CO_2}$ by using the monthly SST and SSS data (Table 3) and monthly air pressure data from the NCEP-DOE Reanalysis 2 (Kanamitsu et al., 2002). We calculated the air-sea $\mathrm{CO_2}$ flux (F) according to Equation 3, such that negative fluxes are into the ocean. The gas transfer coefficient k was determined using the quadratic wind speed (u) dependency of Wanninkhof (2014) (Equation 4). The Schmidt number, Sc, was calculated according to Wanninkhof (2014) and the solubility coefficient for $\mathrm{CO_2}$, K_0, after Weiss (1974).

$$\mathrm{F} = k \cdot K_0 \cdot (f\mathrm{CO_{2,sw}} - f\mathrm{CO_{2,atm}}) \tag{3}$$

$$k = a_q \cdot \langle u^2 \rangle \cdot \left(\frac{Sc}{660} \right)^{-0.5} \tag{4}$$

In our calculations, we used 6-hourly winds of the NCEP-DOE Reanalysis 2 product. The coefficient a_q in Equation 4 is strongly dependent on the used wind product (Roobaert et al., 2018). We determined it to be $a_q = 0.16 \mathrm{cmh^{-1}}$ for the 6-hourly NCEP 2 product following the recommendations of Naegler (2009) and by using the World Ocean Atlas sea surface temperatures (Locarnini et al., 2018). The barrier effect of sea ice on the flux was taken into account by relating the flux to the degree of ice cover following Loose et al. (2009). As the gas exchange in areas that are considered 100% ice covered from satellite images should not be completely neglected, we use a sea ice barrier effect for a 99% sea ice cover in all grid cells where the sea ice coverage exceeded 99%.

3 Results

3.1 Maps of $f\mathrm{CO_2}$

The skill assessment metrics for MLR 1, MLR 2 and MLR 3 are presented in Table 5. It shows the the R^2 and RMSE of the fit, the ME, as well as the average offset and standard deviation to the gridded SOCAT data. The MLRs substantially improve the predictions of the open ocean maps in all studied regions, showing a better average offset and standard deviation to SOCAT v5 and ME than the coarser-resolution open ocean maps (for example: Rödenbeck map: North Sea 0 ± 95 μatm, Norwegian Coast: 2 ± 17 μatm, Barents Sea: 22 ± 40 μatm, Baltic Sea: 4 ± 48 μatm; MLR1: North Sea: 0 ± 26 μatm, Norwegian Coast: 0 ± 16 μatm, Barents Sea: 0 ± 19 μatm, Baltic Sea: 2 ± 42 μatm). In all regions MLR 1 was performing best, showing also the best model efficiency, the highest R^2 and the smallest RMSE of the fit, while MLR 2 and MLR 3 showed a weaker performance. This can be explained by the fact that the Rödenbeck map contains also information about the continental shelf and the Barents Sea, while for MLR 2 the closest open ocean grid cell of Landschützer et al. (2017) was used. MLR 3 showed the weakest performance, which shows the value of using information from the open ocean maps in the regression.

Figure 3 shows, from left to right, the spatial distribution of the average difference between the predicted $f\mathrm{CO_2}$ by MLR1 and the gridded SOCAT v5 data, the Rödenbeck map and the gridded SOCAT v5 data, the difference between MLR 1 and the Rödenbeck map, and, for comparison, between MLR 3 and the SOCAT v5 data. In the North Sea, MLR 1 seems to slightly overestimate the $f\mathrm{CO_2}$ in the constantly mixed region at the entrance of the English channel and the area off the Danish North
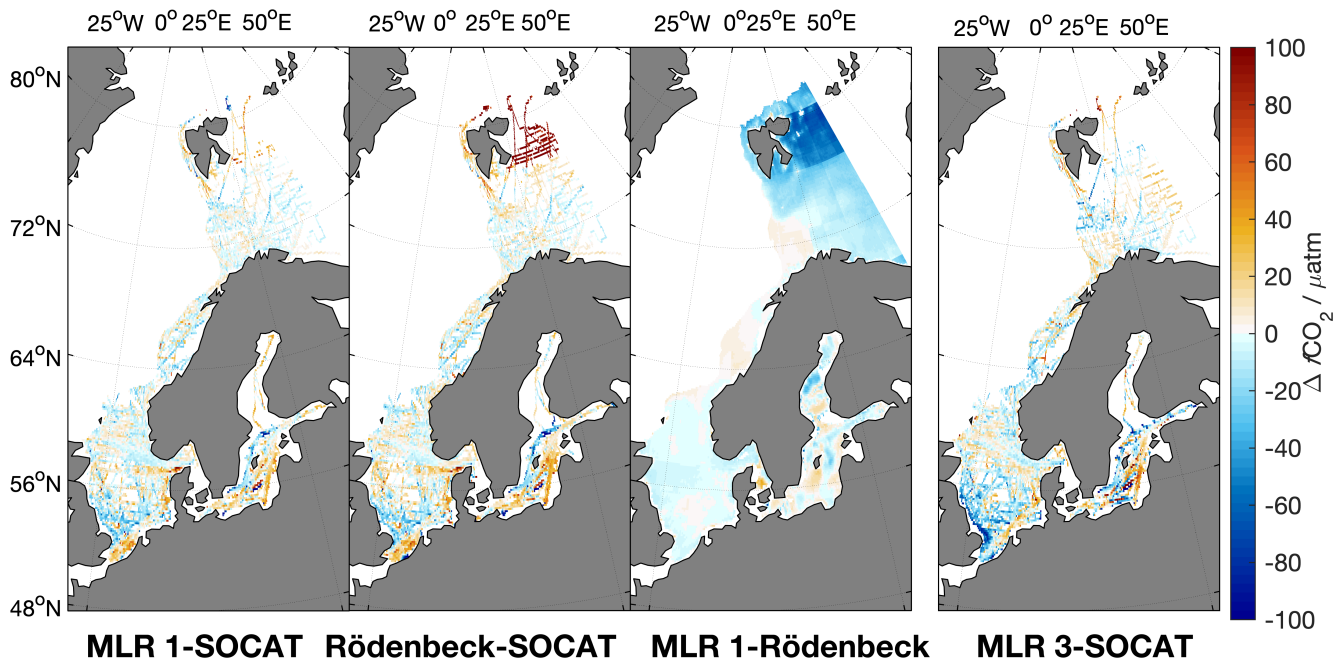
Figure 3. Average regional differences between MLR 1 and gridded SOCAT v5 data, the Rödenbeck map and gridded SOCAT v5 data, MLR 1 and the Rödenbeck map, and MLR 3 and the gridded SOCAT v5 data (from left to right).

Sea coast. In the Baltic, MLR 1 generally describes well the spatial variability in fCO_2. In the Gulf of Finland it usually predicts too low fCO_2 values during May/June while MLR 1 slightly underestimates events of very high fCO_2 in December/January. However, it shows lower spatial biases than the original Rödenbeck map. MLD 2 and 3 are showing much larger differences from SOCAT v5 data, especially in the Baltic Sea and the southern North Sea. Therefore, we will use MLR 1 in the further analysis. An extended validation of the MLR 1 maps can be found in the discussion section.

As most driver data have a smaller resolution than the final maps (see Table 3), the grid of the driver data can be still visible in the final maps. This is specifically the case for the used open ocean pCO_2 maps. Residuals of the original open ocean Rödenbeck map (resolution $5° - 4°$) are clearly visible in the MLR 1 maps as well as the trends and fluxes calculated from these.

Figure 4 shows the monthly averages of fCO_2 produced by MLR 1 for February, May, August and November. In all regions, the highest fCO_2 values occur in the winter, while the lowest fCO_2 occur in summer. The largest seasonal cycle could be observed in the Baltic Sea, where fCO_2 reached well below 200 μatm in mid summer and over 500 μatm during the winter.

Table 5. Statistical evaluation of the MLR 1, MLR 2 and MLR 3 in comparison to the open ocean maps of Rödenbeck et al. (2015) and Landschützer et al. (2017) for each region. The data for the open ocean map of Landschützer et al. (2017) are in parentheses since this is based on an extrapolation of he closed open ocean grid cell towards the coast. The number of grid cells containing data is given behind the region abbreviations.

	R^2 adj	RMSE	ME median	difference to gridded SOCAT v5	
				mean	standard deviation
		/μatm		/μatm	/μatm
North Sea (36170)					
MLR 1	0.7271	25	0.3145	-0.15	26
MLR 2	0.5130	33	0.5789	-0.52	36
MLR 3	0.5331	33	0.4895	-2.4	32
Rödenbeck			0.3522	-0.28	95
(Landschützer)			0.5714	-4.7	103
Norwegian Coast (16014)					
MLR 1	0.7860	16	0.1742	0.46	16
MLR 2	0.5634	22	0.3597	-2.3	24
MLR 3	0.6074	20	0.2436	-0.08	21
Rödenbeck			0.2177	2.0	17
(Landschützer)			0.3294	7.0	23
Barents Sea (13925)					
MLR 1	0.8871	12	0.1069	0.32	19
MLR 2	0.8724	14	0.0986	1.3	68
MLR 3	0.8672	18	0.1082	1.3	24
Rödenbeck			0.2923	22	40
(Landschützer)			0.3364	15	44
Baltic Sea (46810)					
MLR 1	0.9076	39	0.0488	2.2	42
MLR 2	0.6733	66	0.3111	-1.0	68
MLR 3	0.6628	67	0.3027	0.24	69
Rödenbeck			0.1326	4.2	48
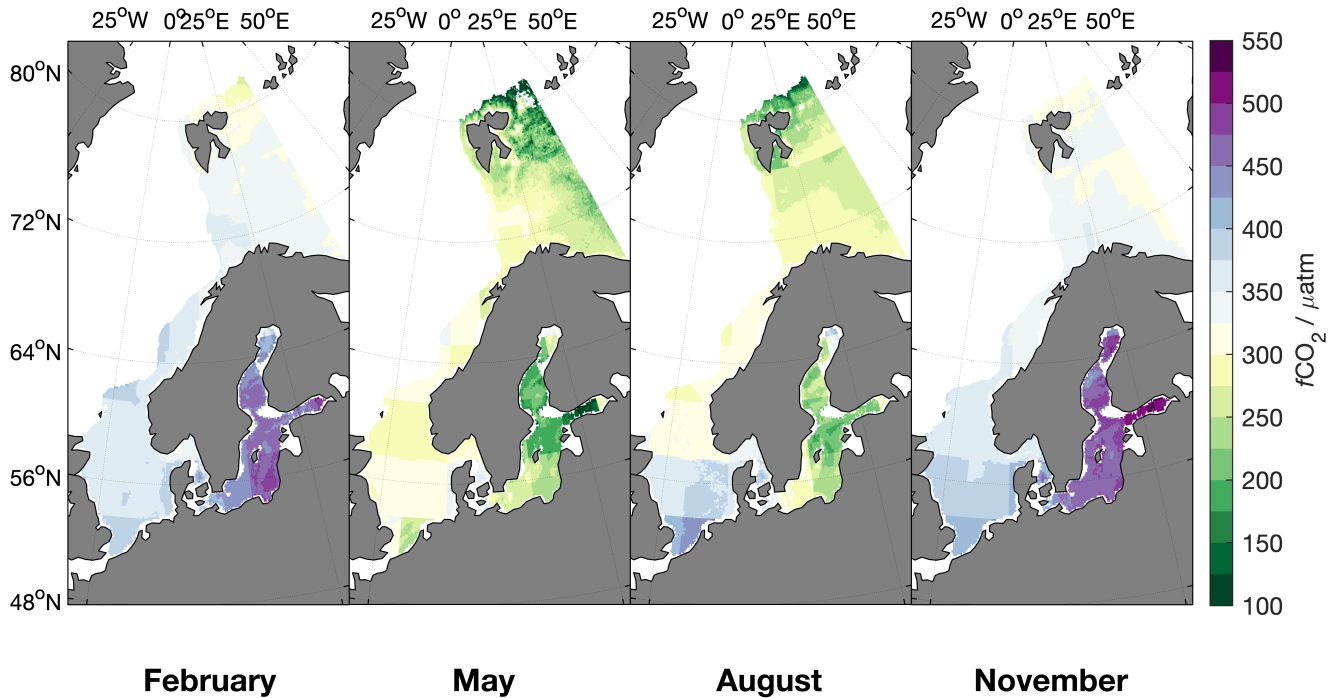
Figure 4. The average $f\mathrm{CO_2}$ of MLR 1 (1998-2016) for one example months in each season (February, May, August and November).

3.2 Maps of pH

The monthly average of pH calculated from MLR 1 $f\mathrm{CO_2}$ is ranging from about 8 during winter to 8.15 during summer in the North Sea and at the Norwegian coast (Figure 5). Towards the Barents Sea the pH maximum increases during summer to 8.2. The pH of 8.00 - 8.15 in regions with a large influence from the Atlantic, such as the northern North Sea and the Norwegian coast, is in good agreement with the range of pH determined for the open North Atlantic (Lauvset and Gruber, 2014; Lauvset et al., 2015). In the North Sea, the pH is in the same range as reported in Salt et al. (2013) and it also shows the same distribution in August/September with higher pH in the northern North Sea and lower pH in the southern part.
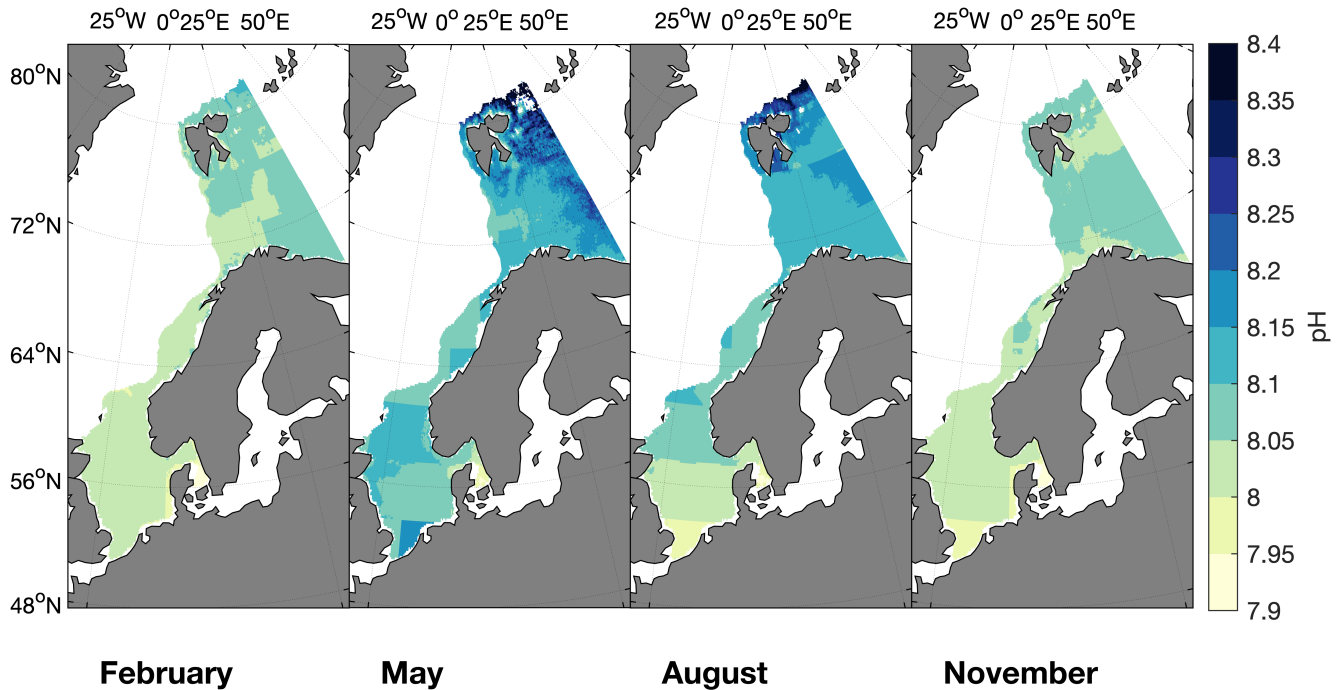
Figure 5. The average pH based on MLR 1 (1998-2016) for one example month in each season (February, May, August and November).

4 Discussion

4.1 Performance of the $p\text{CO}_2$ maps

The performance of the MLR and the produced maps are evaluated in different ways: (1) the R^2 and the RMSE of the fit between the driver data and the gridded observations, (2) the average deviation and its standard deviation, as well as the ME between the produced $f\text{CO}_2$ maps and the gridded observations as a regional average, (3) showing the median deviation between the MLR and the gridded observations on a monthly level, (4) by comparing the data from the $f\text{CO}_2$ maps to observations from two time series stations. (2) - (4) will be shown for both, the time period covered by the driver data (1998-2016) and a prediction of the maps into the years 2017 and 2018. The prediction of the maps into the years 2017 and 2018 will be compared with data from the newest SOCAT release (SOCATv2019) to have a comparison with an independent dataset. Please note that the comparability of the model performance between the different regions is limited. All used statistical parameters are influenced by characteristics that can vary substantially between the different regions, such as range of the data, their variability or the

amount of grid cells with data. Additionally, in a region with many measurements the amount of variability captured by these measurements is most likely larger and, thus will lead to a weaker correlation.

Generally, the uncertainty of MLR 1 are in the same range as in other studies (Laruelle et al., 2017; Yasunaka et al., 2018) mapping coastal $f\text{CO}_2$ dynamics: 25 μatm in the North Sea, 16 μatm along the Norwegian Coast, 12 μatm in the Barents Sea,
5 and 39 μatm in the Baltic Sea (based on the RMSE in Table 5). In the Baltic Sea, which has a large variability in itself, Parard et al. (2016) obtained lower standard deviations through dividing the area in smaller sub-regions.

The seasonal differences between MLR 1 and the SOCAT v5 data for each region are shown in Figure 6. This comparison shows a very good agreement. For MLR 1, the seasonal variations of the median bias are small in the North Sea, along the Norwegian coast and in the Baltic Sea. In the Barents Sea, however, the bias varies seasonally. Here, MLR 1 slightly
10 underestimates the $f\text{CO}_2$ in winter and early spring, while it overestimates the $f\text{CO}_2$ in summer. In all other regions, the median seasonal bias is smaller than the uncertainty of the maps. The larger seasonal bias in the Barents sea is most likely caused by the larger seasonal bias in the number of available observations. There is no data available in October, December and January.

When comparing all observations from the years 2017 and 2018 to the predictions by the MLR 1, we find a good agreement
15 in the North Sea (2 ± 20 μatm) and no seasonal bias (Figure 7). In the other regions, the agreement is somewhat reduced compared to the years 1998-2016 (-9 ± 39 μatm (Norwegian Coast), -5 ± 29 μatm (Barents Sea) and 28 ± 58 μatm (Baltic Sea)). In these regions we also observe a seasonal bias in the years 2017 and 2018. At least for the Baltic Sea this could be a result of the extraordinarily warm and dry summer in 2018, that lead to very low $f\text{CO}_2$ values in the Baltic Sea (see Figure 8 and the data in SOCAT Bakker et al. (2016)). Please note, that for this comparison the MLR was extrapolated in time. Only
20 observations until December 2016 were used to produce the MLR. Therefore accuracy of the maps itself is reduced.

In a second test to investigate to which extent MLR 1 can reproduce observations we compared the MLR output with time series data from two voluntary observing ship lines in two very different regions with a good data coverage: M/V Nuka Arctica in the northern North Sea (0-2°E, 58-60°N) and M/V Finnmaid in the Baltic Sea (23-24°E, 59-60°N) (Figure 8). To every observation we assigned the related value of MLR 1. The agreement between the MLR 1 and the observations is very good.
25 MLR 1 reproduces the general seasonality and some of the interannual variability, also in the years 2017 and 2018, of which the observations were not used in the regression.

When performing interpolation exercises it is always important to be aware of the fact that the resulting maps might come with biases and do not represent all regions equally well. While the here presented maps give a good general overview about the surface ocean $f\text{CO}_2$ variability in regions with a relatively large amount of data, the reliability, however, is limited in
30 those regions where the data coverage is more scarce. This is especially the case, when the region with scarce data coverage is showing different characteristics in, for example, temperature and salinity, compared to the rest of the region. One such example is the Gulf of Bothnia in the Baltic Sea region where almost all data used to derive the MLR is from south of 60°N i.e. not in the Gulf of Bothnia, but in the Baltic Proper and western Baltic Sea (Figure 2). The MLR method can also lead to unrealistic extreme values and even negative $f\text{CO}_2$. Some such values occur in the northeastern Barents sea as well as in
35 some parts of the Baltic Sea (about 0.01% of the grid cells in each region). As pH cannot be calculated for negative $f\text{CO}_2$, we
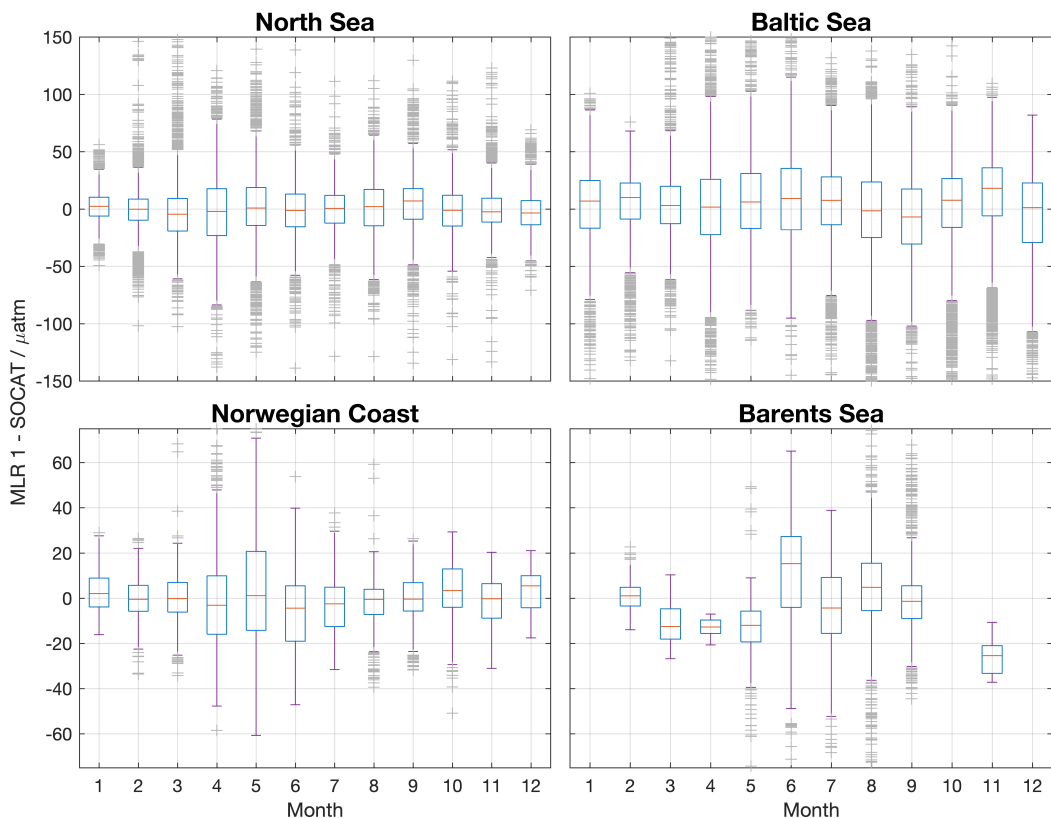
Figure 6. Boxplots showing the median deviation of MLR 1 from the gridded SOCAT 5 data for each region (red line). The boxes show the respective 75% percentiles. 99% of the data lays within the range of the purple whiskers. Extremes are shown as gray crosses.

excluded all negative $f\mathrm{CO_2}$ values for the calculation of pH. Excluding the negative values resulted in a change of the average $f\mathrm{CO_2}$ of 0.05 μatm (Baltic Sea) and 0.3 μatm (Barents Sea) so they are of negligible importance for the flux estimates. While the negative values are easy to spot and discard there are most likely more unrealistically low values in spring and summer data in the very north and northeastern Barents Sea as well as some parts of the Baltic Sea. However, there are no data available in
5   SOCAT v5 or elsewhere available to validate this.

All regions with questionable $f\mathrm{CO_2}$ are also questionable in their pH data. There is a number of very high pH in the Barents Sea, that are associated with also very low $f\mathrm{CO_2}$ that might not be realistic. In addition, estimated pH values in low salinity regions where the actual alkalinity-salinity deviates strongly from the Nondal et al. (2009) one used here (e.g. river mouths in the southern North Sea or the Skagerrak), should be interpreted with caution.
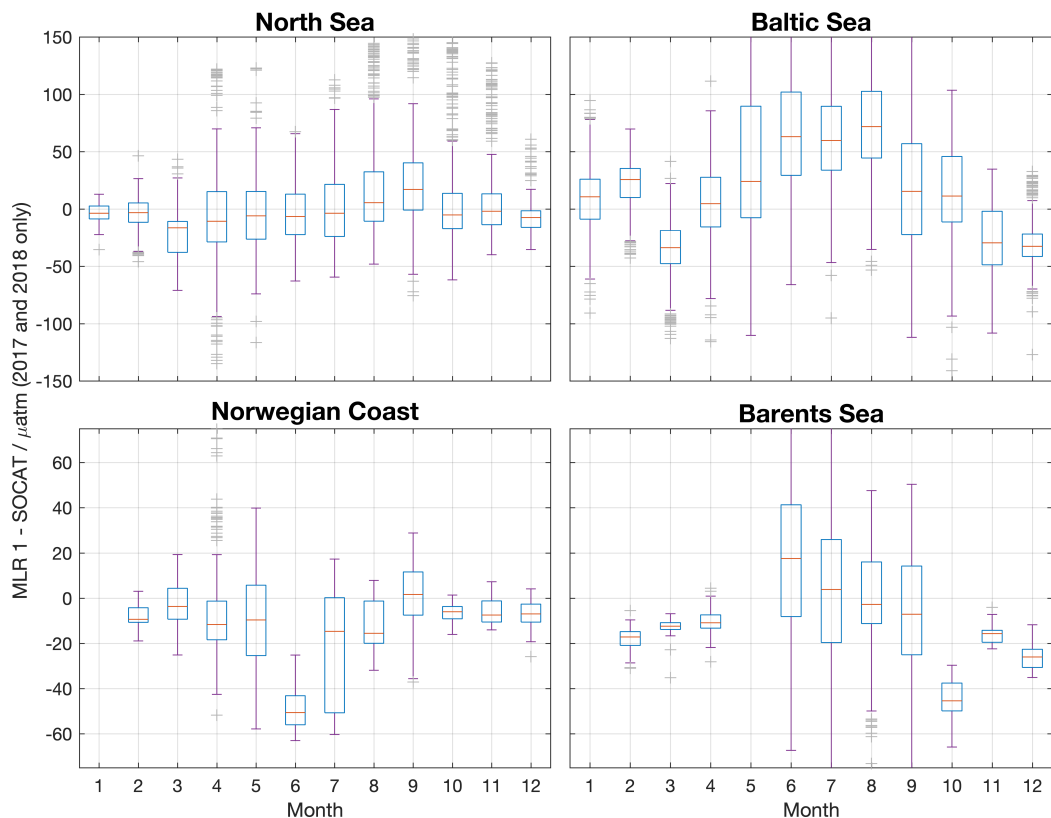
Figure 7. Boxplots showing the median deviation of MLR 1 (based on observations until 2016) predicted and measured $f\text{CO}_2$ values in 2017 and 2018. The boxes show the respective 75% percentiles. 99% of the data lays within the range of the purple whiskers. Extremes are shown as gray crosses. The number of grid cells with data available were: North Sea: 5047 , Norwegian Coast: 1543, Barents Sea: 2312, Baltic Sea: 5414.

4.2 Trends in $f\text{CO}_2$ and pH

The trends in surface ocean $f\text{CO}_2$ in coastal regions are often difficult to assess because of the scarcity of the data relative to the highly dynamical character of these regimes and their large interannual variability. One issue is that the start of the productive season can range from February to April even within a small area, such that even restricting the analysis to specific seasons

5   (e.g. winter) can be challenging. However, due to lack of data, especially winter data, most observational studies are based on repeated sections during summer. Further, the fact that these measurements typically do not take place every year, adds even more uncertainty to the estimated trend, as the interannual variability can mask the trend signal.

The monthly maps of $f\text{CO}_2$ from 1998 to 2016 enable us now to estimate the trend in surface ocean $f\text{CO}_2$ for the entire region, equally distributed over the seasons (Figure 9, left). All trends were computed by using deseasonalized data. The

10   interannual variability of the trend estimates in each region is shown in the panels on the right hand side in Figure 9. Based
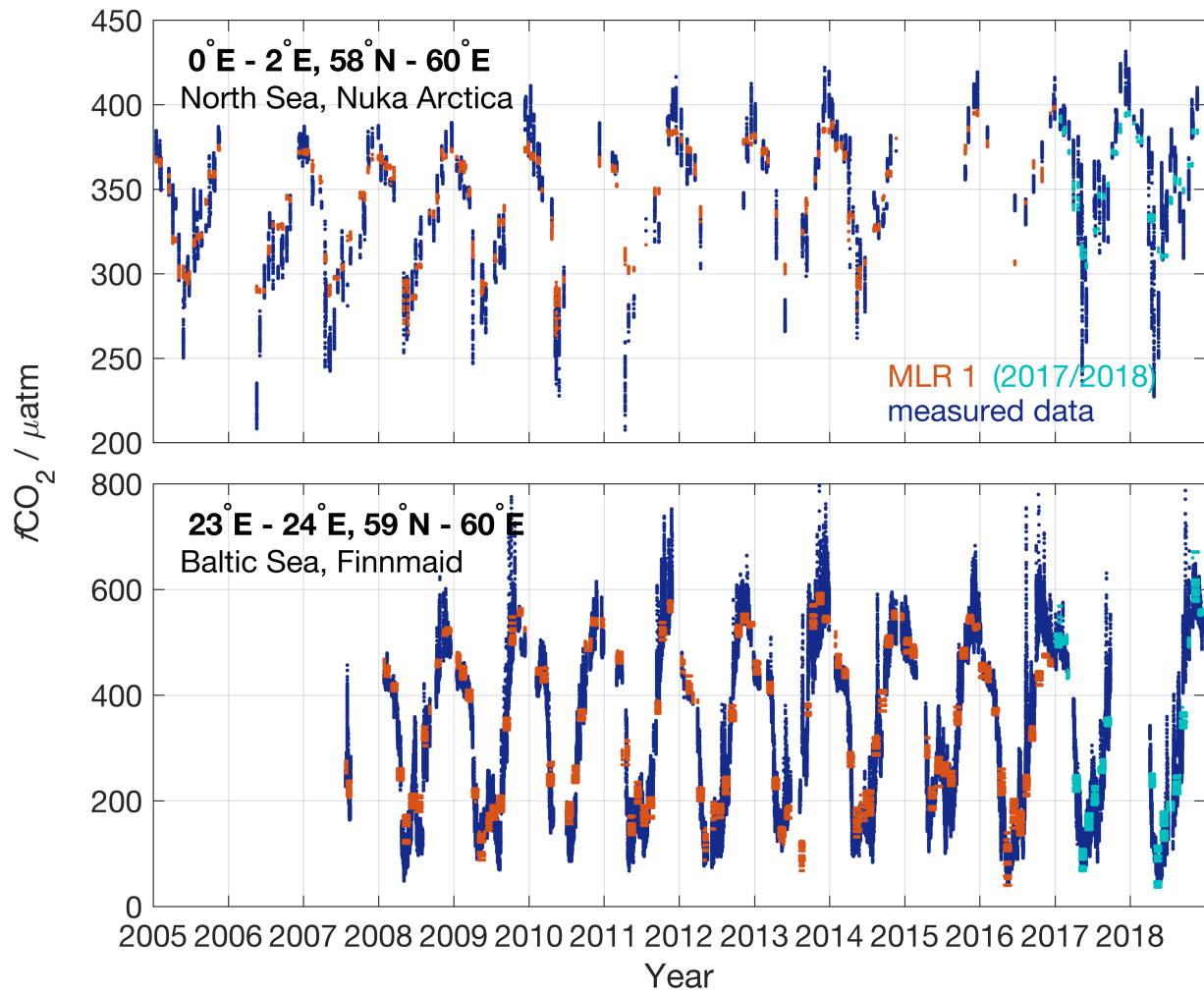
Figure 8. Time series of VOS data from Nuka Arctica (upper panel, blue) and Finnmaid (lower panel, blue) compared with MLR 1 at the same location (red). In light blue the predictive MLR output for the years 2017 and 2018 is shown.
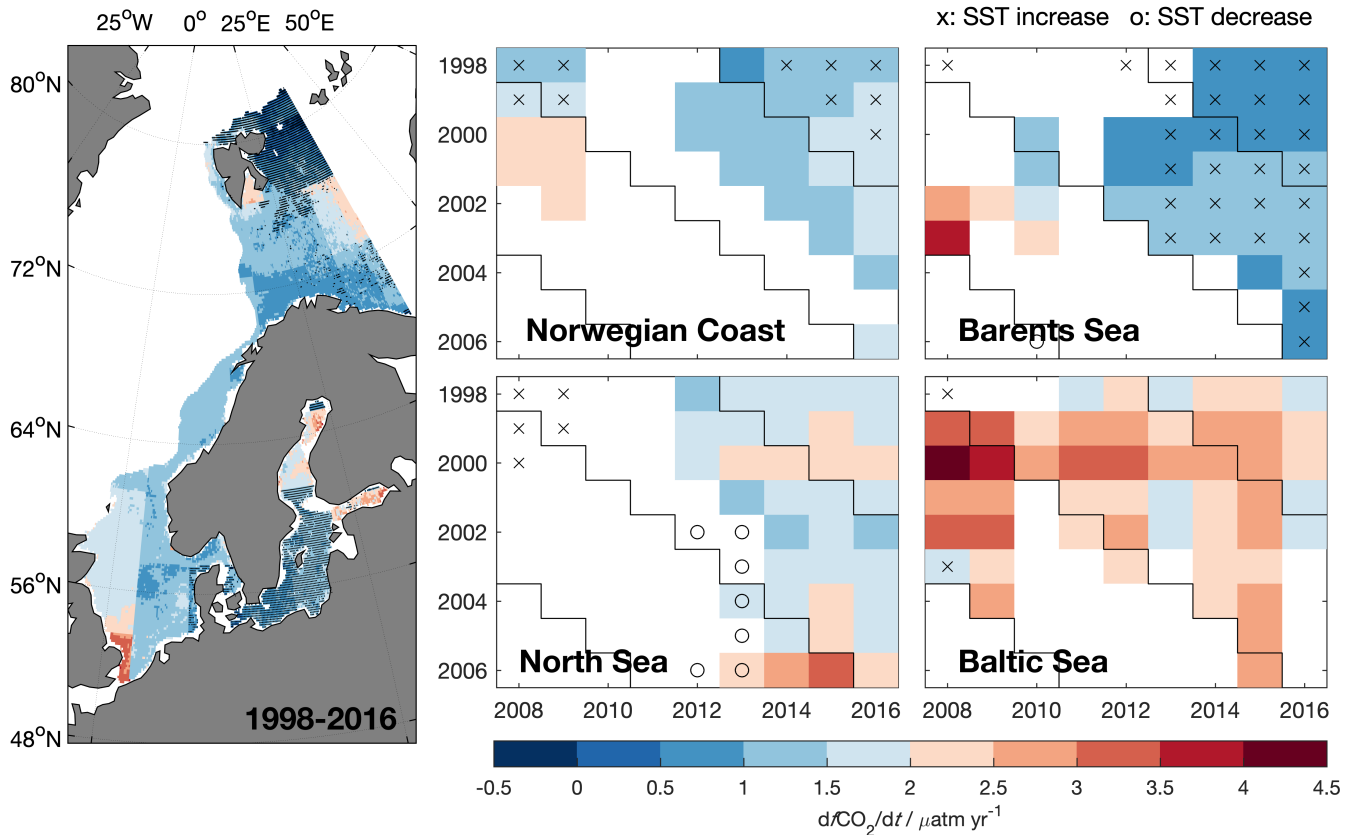
Figure 9. The trend in surface ocean $f\mathrm{CO}_2$ estimated from deseasonalized $f\mathrm{CO}_2$. The left hand panel show the spatial distribution of the trend over the time period from 1998 to 2016. Grid boxes without a significant trend are denoted with a black dot. On the right hand the influence of the time range on the average trend is shown for the four regions. Non significant trends were left blank. Significant trends in sea surface temperature are indicated with crosses/circles.

on the linear regression the significant trends in $f\mathrm{CO}_2$ have an average uncertainty of 0.5 μatm/yr (North Sea), 0.4 μatm/yr (Norwegian Coast), 0.4 μatm/yr (Barents Sea), and 0.7 μatm/yr (Baltic Sea), while the shorter time periods shown have a higher and the longer time periods a lower uncertainty. For pH trends the average uncertainty of the regression is $5 \cdot 10^{-4}$ (North Sea) and $7 \cdot 10^{-4}$ (Norwegian Coast and Barents Sea).

5   In most of the regions addressed in this study, the trend in the surface ocean is lower than the trend in atmospheric $x\mathrm{CO}_2$ (global average 2.02 ppm yr^{-1} ("Cooperative Global Atmospheric Data Integration Project", 2015)). Trends exceeding the atmospheric values in the period from 1998 to 2016 can only be observed at the entrance of the English Channel, in Storfjorden/Svalbard, the Gulf of Finland and the Gulf of Bothnia ($2.5 - 3$ μatm yr^{-1}). It has to be noted that there was almost no measured $f\mathrm{CO}_2$ as MLR input in neither Storfjorden nor the Gulf of Bothnia. Therefore, these trends should be handled with

Table 6. $f\mathrm{CO}_2$ trend calculated from gridded, deseasonalized SOCAT v5 observations.

Region	Latitude / $^\circ$N	Trend / μatm yr^{-1}
North Sea, South	51 - 54.5	3.2 ± 1.3
North Sea, Center	54.5 - 58	1.43 ± 0.21
North Sea, North	58 - 62	2.320 ± 0.089
Norwegian Coast, South	62 - 68	2.12 ± 0.19
Norwegian Coast, North	68 - 73	1.426 ± 0.099
Barents Sea, South	69 - 74	1.31 ± 0.30
Barents Sea, North	74 - 85	1.01 ± 0.22
Baltic Sea, South	54 - 56	2.05 ± 0.12
Baltic Sea, North	56 - 61	1.84 ± 0.21

care. The western North Sea has a trend that is only slightly lower than the trend in the atmosphere ($1.5-2$ μatm yr^{-1}), while the trends in the eastern North Sea, along the Norwegian coast and in the Barents Sea are somewhat lower (0.5-1.5 μatm yr^{-1}). In the North Sea this is consistent with a recent study directly based on observations Omar et al. (2019). These low trends will result in an increase in the strength of the ocean carbon sink with time.

5   The northern European shelf is a region with a high data density. In order to validate the general patterns of $f\mathrm{CO}_2$ trends we estimated the $f\mathrm{CO}_2$ trends also from the SOCAT v5 observations, that were used to produce the MLR (Table 6). We gridded and deseasonalized the SOCAT v5 data and divided the entire region into 9 subregions. A figure showing the fits and the data coverage can be found in Appendix A. These observation based trends show similar general patterns as those based on our maps (Figure 9, 1998-2016): (1) largest trends in the southern North Sea, (2) decreasing towards the North with trends around

10   the atmospheric trend in the northern North Sea and trends around 1 μatm yr^{-1} in the Barents Sea, (3) close to atmospheric trends in the Baltic Sea.

     The observation that large subareas (the Baltic Sea or along the shore of the western North Sea) did not show a significant trend can be explained by the fact, that coastal sea systems, especially enclosed areas as the Baltic Sea, experience a high anthropogenic pressure. Anthropogenic impacts other than rising atmospheric CO_2 concentrations influencing the ocean carbon

15   system and the bloom properties such as the nutrient load of rivers can effect coastal ecosystems through eutrophication. This will result in lower $f\mathrm{CO}_2$ in summer and higher $f\mathrm{CO}_2$ in winter (Borges and Gypens, 2010; Cai et al., 2011). Another important process that influences the carbon system in the Baltic Sea are inflow events from the North sea. In between such events, CO_2 accumulates in deeper water layers causing an increasing gradient of dissolved inorganic carbon (DIC) across the halocline. Whenever deep winter mixing occurs, this will then lead to a large increase of surface $f\mathrm{CO}_2$ because of the input of DIC rich

waters from below. Another reason is the observed change in alkalinity with time which effects the $f\text{CO}_2$ though changes in the buffer capacity of the inorganic carbon system (Müller et al., 2016).

One reason for a trend smaller than in the atmosphere can be a shift in the bloom onset. For example, in the North Sea a significant drawdown in $f\text{CO}_2$ has been observed as early as February in some years, but there is also a large variability (Omar et al., 2019). The bloom timing and onset in the North Sea after the 1990s has been shown to be mainly triggered by the spring-neap tidal cycle and the air temperature (Sharples et al., 2006). The bloom timing and onset was found to be significantly earlier in the 2010s compared to the previous decades (Desmit et al., 2020). Even if the trend in winter $f\text{CO}_2$ was following the atmospheric $x\text{CO}_2$ increase, such a change in bloom timing and onset would lead to a trend lower than the atmospheric when averaging over the entire year. The hypothesis, that an earlier or more intense bloom onset is responsible for the relatively low trends in the North Sea is supported by looking at the contributions of the different months to the overall trend. Figure 10 shows the trend for each month in the four different regions.

When looking at the interannual variability, it becomes obvious that the trend in the North Sea is slightly smaller than the atmospheric CO_2 trend. In contrast, the Norwegian coast and the Barents Sea experience a robust trend much lower than the atmospheric trend (Norwegian Coast: $1-1.5$ μatm yr^{-1}, Barents Sea: around 1 μatm yr^{-1}). Here we can also see a stable pattern of warming over time scales of 10 to 15 years. The warming in itself would result in an increase of $f\text{CO}_2$ with time, in addition to the atmospheric forcing. As we are observing a trend smaller than the atmospheric trend, temperature effects can't be the driver here. The lower trend stems most likely from an earlier onset of spring bloom. It has been shown that the atlantification and the reduced ice coverage of the Barents sea leads to a longer productive season, and this will result in more months with strong undersaturation in CO_2 (Oziel et al., 2016). In the Baltic Sea the pattens are different. Here the variability is much larger, while most of the time periods show a trend larger than the atmospheric trend ($3-3.5$ μatm yr^{-1}). Although slightly smaller our results broadly agree with trend estimates based on measurements of 4.6 - 6.1 μatm yr^{-1} over 2008-2015 (Schneider and Müller, 2018). Finally, it also needs to be noted that the uncertainty of the $f\text{CO}_2$ maps was highest in the Baltic Sea. This makes it also more difficult, if not impossible, to properly detect these small trends.

For pH, the trend in most regions is around -0.002 yr^{-1} (Figure 11). A expected, regions with the strongest trend in $f\text{CO}_2$ also show the highest trend in pH, such as the southern North Sea. The trend in the northern North Sea and along the Norwegian Coast is in good agreement with the pH trends found in studies focusing on the open Atlantic Ocean (-0.0022 yr^{-1} (Lauvset and Gruber, 2014)) and the North Atlantic and Nordic Seas (-0.002 yr^{-1} (Lauvset et al., 2015)).

4.3 CO$_2$ disequilibrium and flux

The average sea-air CO_2 disequilibrium ($\Delta f\text{CO}_2 = f\text{CO}_{2,\text{sea}} - f\text{CO}_{2,\text{atm}}$) is shown in Figure 12. The only region showing an average supersaturation is the southern North Sea. Towards the north, the surface ocean becomes more and more undersaturated, with lowest values in the Barents Sea. The values we found in the Barents Sea (-60 to -80 μatm in the southern Barents Sea and less than -100 μatm around Svalbard) are in generally in agreement those estimated by Yasunaka et al. (2018). The seasonal cycle of $\Delta f\text{CO}_2$ follows a mainly biologically driven pattern with higher values in the winter and lower values from April to August. The seasonal cycle is largest in the Baltic and smallest in the Barents Sea.
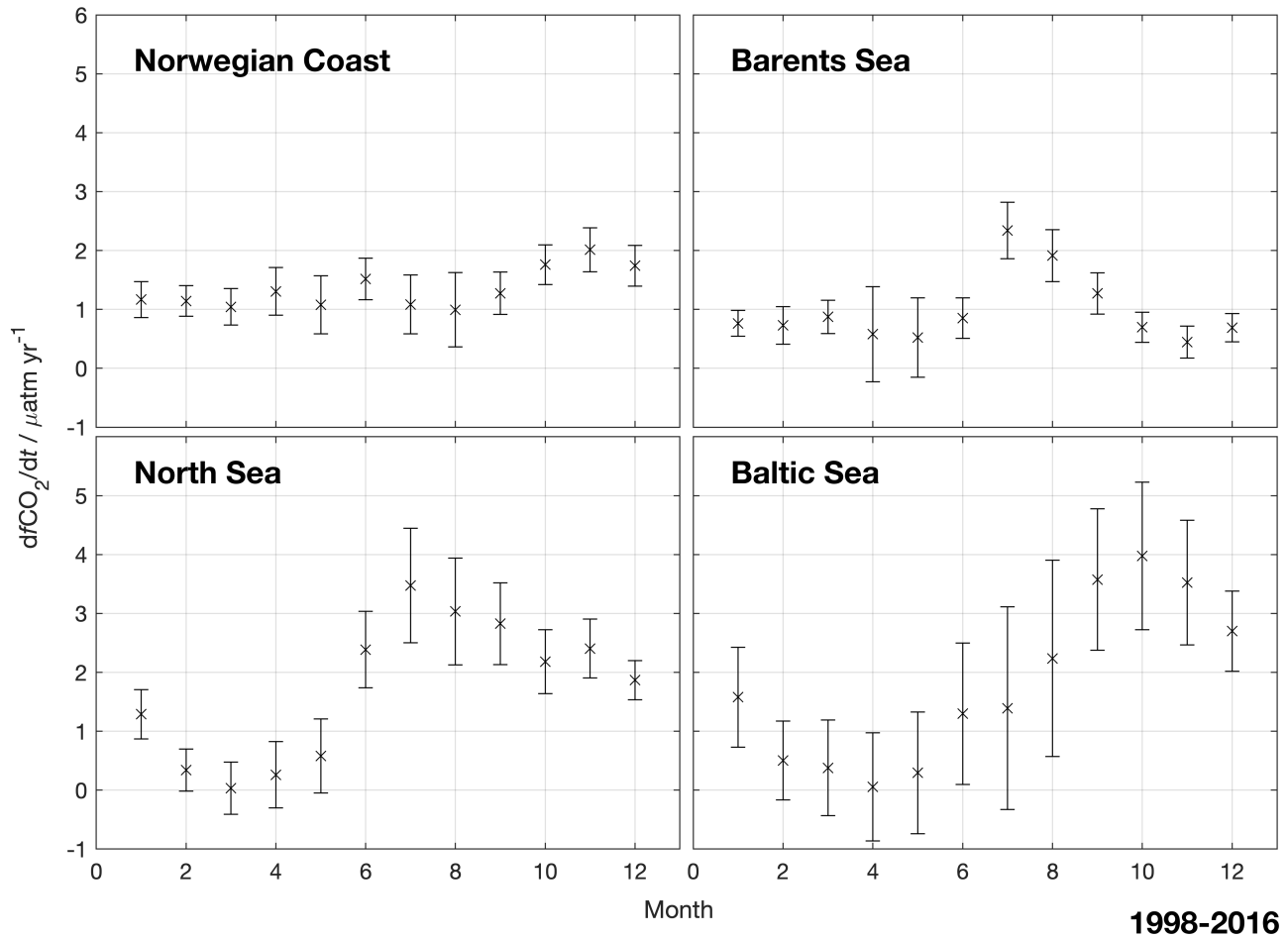
Figure 10. The trend in surface ocean fCO$_2$ estimated resolved per month (1998 to 2016).

The sea-air CO$_2$ fluxes (Figure 13) show that most regions are a net and increasing sink for CO$_2$. The only source net regions are the southern North Sea and the Baltic Sea. The two different regimes in the North Sea with the southern, nonstratified part being a source and the northern temporarily stratified part a sink for CO$_2$, have been described in the literature before (Thomas et al., 2004). However, there is a large interannual variability in the fCO$_2$ disequilibrium (Omar et al., 2010). This is reflected in the fact that studies based on different years find conflicting results regarding the direction of the flux (Schiettecatte et al., 2007; Thomas et al., 2004). This large interannual variability can also be found in our maps. During some years larger parts of the North Sea were a net source, while during other years also the southern North Sea acted as net sink.

The seasonal variations in the air-sea flux are driven by a combination of the changes in the disequilibrium, the wind strength, and the ice cover. As there is less wind during summer, when the disequilibrium is large, but a smaller disequilibrium during winter, when the wind strength is high, the seasonal variability is often less clear than that of e.g. the disequilibrium. This
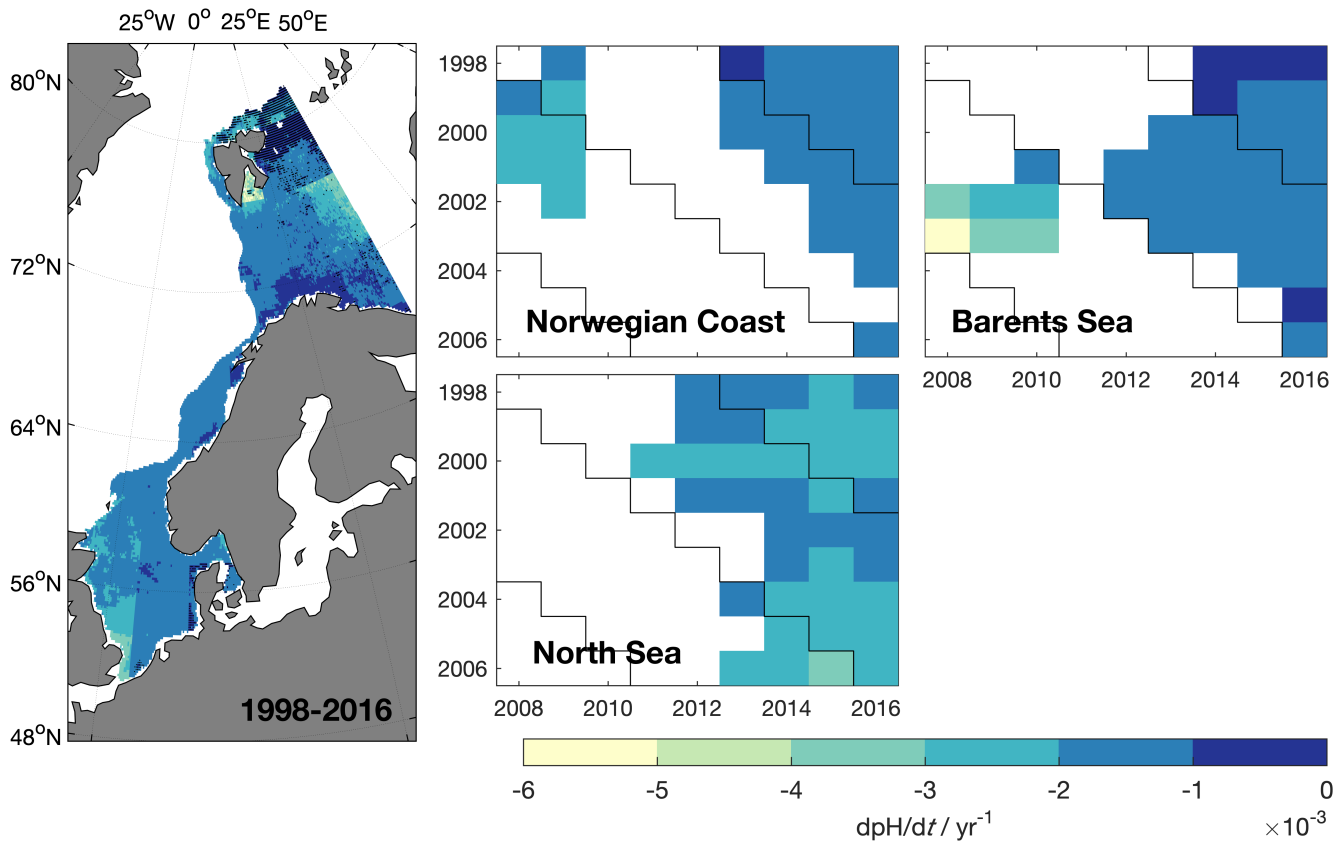
Figure 11. The trend in surface ocean pH estimated from deseasonalized pH. On the left hand the spatial distribution of the trend over the time period from 1998 to 2016 is shown. Grid boxes without a significant trend are denoted with a black dot. On the right hand the influence of the time range on the average trend is shown for the four regions. Non significant trends were left blank.

can be seen in the Barents Sea and Norwegian Coast. Yasunaka et al. (2018) found the seasonal and interannual variation in the Barents Sea and the Norwegian Sea mostly corresponded to the wind speed and the sea ice concentration. In contrast to that we see the strongest dependence on the air-sea disequilibrium. However, even though we don't find the same seasonality, considering the error margin and the small amplitude of the seasonality, our average fluxes fit well with those reported by Yasunaka et al. (2018) of -8 to -12 mmol m^{-2} d^{-1} (Barents Sea) and -4 to -8 mmol m^{-2} d^{-1} (Norwegian Coast). In the North Sea there is almost no net flux during winter, as the surface ocean is more or less in equilibrium with the atmosphere. In the Baltic Sea, we can see high fluxes into the atmosphere during winter as here a large oversaturation coincides with high wind strengths. This is also why the Baltic Sea is a net source regions. Although Parard et al. (2017) did find slightly smaller fluxes (+15 mmol m^{-2} d^{-1} during winter and -8 mmol m^{-2} d^{-1} during summer), the annual air-sea CO$_2$ fluxes are in good agreement (0 to +4 mmol m^{-2} d^{-1} between 1998 and 2011).
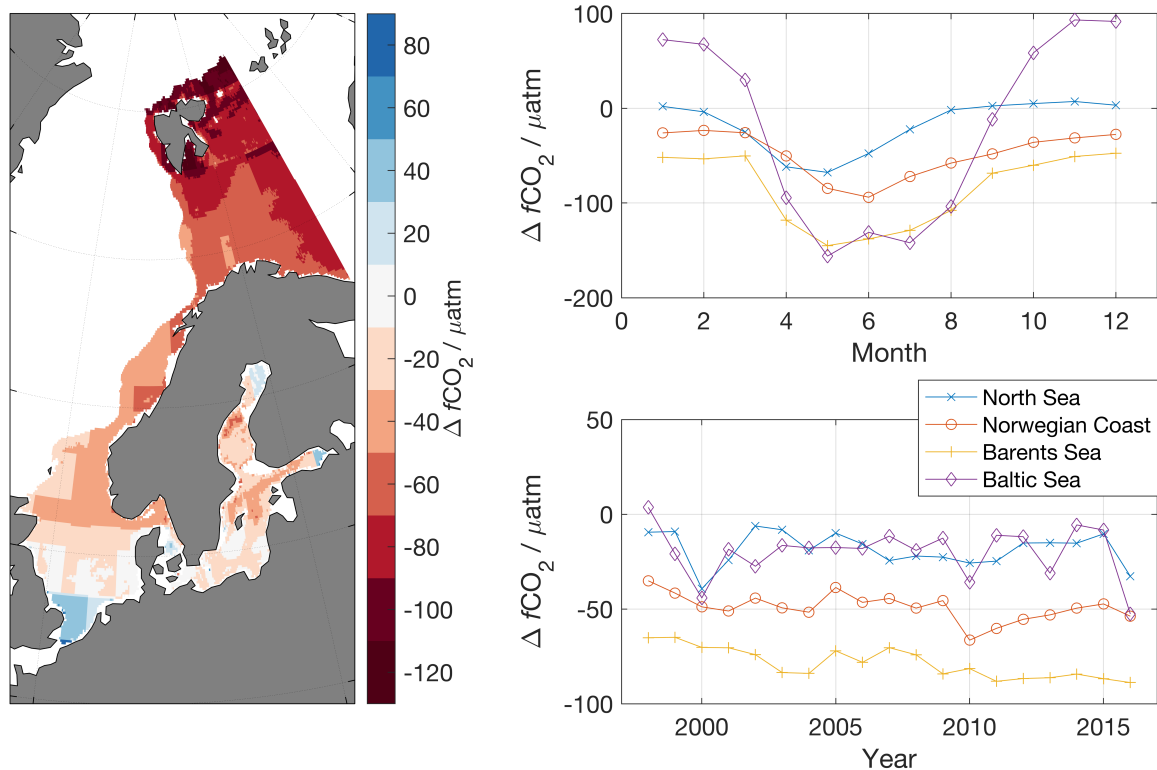
Figure 12. The average air-sea CO_2 disequilibrium over the period 1998-2016 (left hand panel, red colors indicate average undersaturation, while blue colors indicate average oversaturation). For every region average disequilibria are shown as seasonal averages (right side, upper corner) and time-series of annual disequilibria (right side, lower corner). Blue line: North Sea, red line: Norwegian coast, yellow line: Barents Sea, purple line: Baltic Sea

The uncertainty in the calculated fluxes is a result of the uncertainties in the fCO_2 observations, ΔfCO_2 maps, the gas exchange parameterization and the wind product. The uncertainty of the ΔfCO_2 is mostly driven by the uncertainty of the MLR, resulting in an error between 12 μatm and 39μatm, according to the RMSE values of MLR1 for the different regions (Table 5). A number of studies addresses on the uncertainty of gas exchange parameterizations and the wind products (Couldrey et al., 2016; Gregg et al., 2014; Ho and Wanninkhof, 2016). For this study, we apply an uncertainty of the gas transfer velocity of 20% (Wanninkhof, 2014). This will result in an uncertainty of the air-sea flux of about 2 mmol C d^{-1} m^{-2}. It has to be kept in mind, that the absolute uncertainty in k increases with increasing wind speed, but that the uncertainty in the wind speed has largest influence in summer when also the disequilibrium is large. In contrast to that the uncertainty in ΔfCO_2 will cause larger errors in winter, when the wind speeds are high.
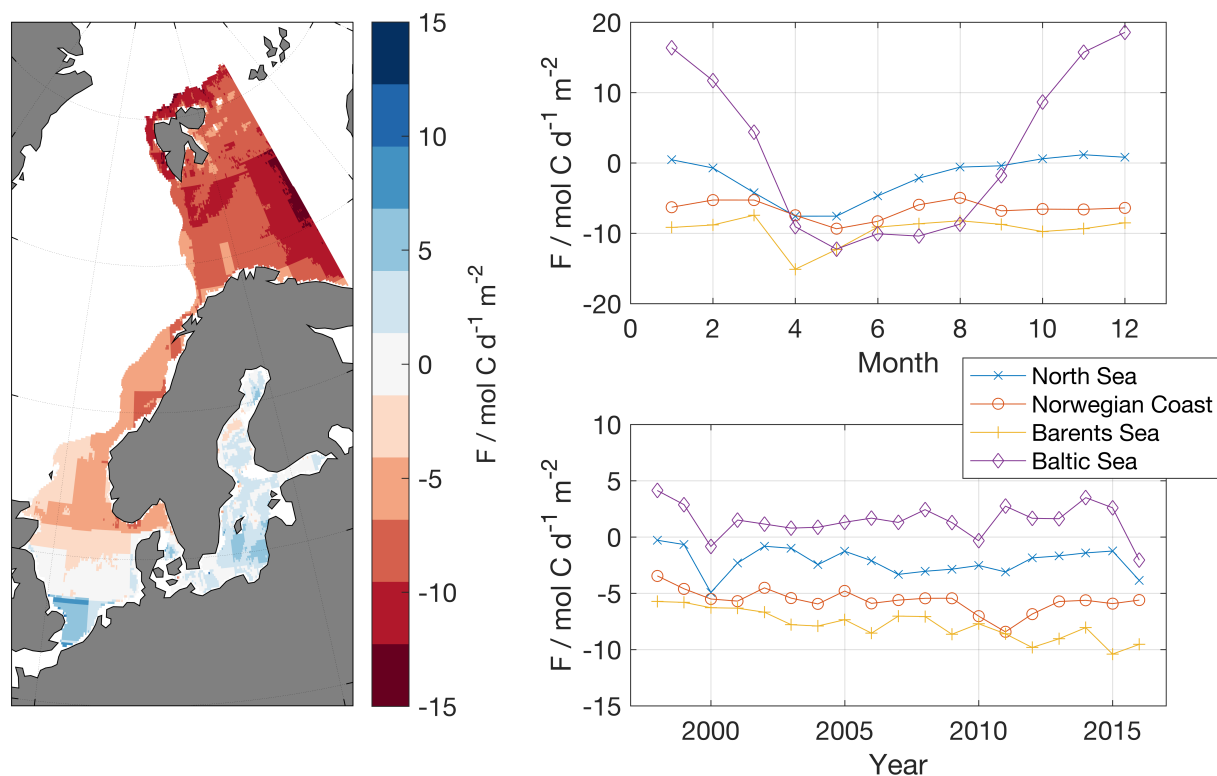
Figure 13. The average air-sea CO_2 flux over the period 1998-2016 (left hand panel, red colors indicate sink regions, while blue colors indicate source regions). For every region average fluxes are show as seasonal averages (right side, upper corner) and timeseries of annual fluxes (right side, lower corner).

5 Conclusions

The MLR approach presented in this work is a relatively easy and straight forward method to produce monthly $f\mathrm{CO_2}$ maps with a high spatial resolution in coastal seas. Using available open ocean maps did improve the coastal maps significantly. The maps reproduce nicely the main spatial and temporal patterns that can also be found in observations in the different regions for
5 both $f\mathrm{CO_2}$ and pH. The surface seawater $f\mathrm{CO_2}$ trends were mostly lower than the atmospheric trends and also lower than the trends found in the open North Atlantic. We did find the northern European shelf to be an increasing net sink for CO_2. Only the Baltic Sea is a net source region. This method clearly has the potential to be extended to a larger region. However, it should be handled with care in regions with only a small number of observations as the MLR can lead to unrealistic values.

Longterm observations with a high temporal resolution are extremely important for developing maps such as presented here.
10 While a decent spatial coverage exists for the open North Atlantic, most coastal regions are still undersampled. This is in particular the case for higher latitudes and in the Arctic. To further understand and interpret the trends on $f\mathrm{CO_2}$ and pH it

is necessary to increase our knowledge and understanding of the interaction of primary production, respiration in the water column and the sediments, mixing and gas exchange and their influence on the carbon cycle.

While MLR derived sea surface provides coherent picture of the entire region, they have clear limitations and should be interpreted with caution in regions with few or none observations. Both, for producing high quality maps, as well for their validation a large number of observations is essential.Also, observations of second parameter of the carbon system would be beneficial for deriving pH maps. This will help to reduce and quantify the error introduced by estimating alkalinity from salinity. In addition to that, our work neglects the areas closest to land due to unavailability of CO_2 data and reanalysis products in those areas. For adding their contribution to the flux estimates, new platforms specialized on measurements directly at the land-ocean interface need to be developed.

Data availability. The dataset is available under: https://doi.org/10.18160/939X-PMHU.

Appendix A: Trend in surface ocean $f\mathrm{CO_2}$ observations

Competing interests. The authors declare no competing interests.

Acknowledgements. First of all, we want to thank everyone involved in the collection and quality control of surface ocean CO_2 data. The Surface Ocean CO_2 Atlas (SOCAT) is an international effort, endorsed by the International Ocean Carbon Coordination Project (IOCCP), the Surface Ocean Lower Atmosphere Study (SOLAS) and the Integrated Marine Biosphere Research (IMBeR) program, to deliver a uniformly quality-controlled surface ocean CO_2 database. The many researchers and funding agencies responsible for the collection of data and quality control are thanked for their contributions to SOCAT. We used NCEP Reanalysis 2 data provided by the NOAA/OAR/ESRL PSD, Boulder, Colorado, USA, from their web site at https://www.esrl.noaa.gov/psd/. This study has been conducted using E.U. Copernicus Marine Service Information. This research was funded by the Research Council of Norway projects ICOS-Norway (Grant 245927) and Nansen Legacy (Grant 276730); the VERIFY project (European Union's Horizon 2020 research and innovation program grant agreement No 776810); and BONUS Integral.

North Sea, South
51°N - 54.5°N
(3.2 ± 1.3) μatm yr^{-1}

North Sea, Center
54.5°N - 58°N
(1.43 ± 0.21) μatm yr^{-1}

North Sea, North
58°N - 62°N
(2.320 ± 0.089) μatm yr^{-1}

Norwegian Coast, South
62°N - 68°N
(2.12 ± 0.19) μatm yr^{-1}

Norwegian Coast, North
68°N - 73°N
(1.426 ± 0.099) μatm yr^{-1}

Barents Sea, South
69°N - 74°N
(1.31 ± 0.30) μatm yr^{-1}

Barents Sea, North
74°N - 85°N
(1.01 ± 0.22) μatm yr^{-1}

Baltic Sea, South
54°N - 56°N
(2.05 ± 0.12) μatm yr^{-1}

Baltic Sea, North
56°N - 61°N
(1.84 ± 0.21) μatm yr^{-1}

SOCAT observations
Linear regression

gridded fCO$_2$ deseasonalized / μatm

Year

References

Bakker, D. C. E., Pfeil, B., Landa, C. S., Metzl, N., O'Brien, K. M., Olsen, A., Smith, K., Cosca, C., Harasawa, S., Jones, S. D., Nakaoka, S.-i., Nojiri, Y., Schuster, U., Steinhoff, T., Sweeney, C., Takahashi, T., Tilbrook, B., Wada, C., Wanninkhof, R., Alin, S. R., Balestrini, C. F., Barbero, L., Bates, N. R., Bianchi, A. A., Bonou, F., Boutin, J., Bozec, Y., Burger, E. F., Cai, W.-J., Castle, R. D., Chen, L., Chierici, M., Currie, K., Evans, W., Featherstone, C., Feely, R. A., Fransson, A., Goyet, C., Greenwood, N., Gregor, L., Hankin, S., Hardman-Mountford, N. J., Harlay, J., Hauck, J., Hoppema, M., Humphreys, M. P., Hunt, C. W., Huss, B., Ibánhez, J. S. P., Johannessen, T., Keeling, R., Kitidis, V., Körtzinger, A., Kozyr, A., Krasakopoulou, E., Kuwata, A., Landschützer, P., Lauvset, S. K., Lefèvre, N., Monaco, C. L., Manke, A., Mathis, J. T., Merlivat, L., Millero, F. J., Monteiro, P. M. S., Munro, D. R., Murata, A., Newberger, T., Omar, A. M., Ono, T., Paterson, K., Pearce, D., Pierrot, D., Robbins, L. L., Saito, S., Salisbury, J., Schlitzer, R., Schneider, B., Schweitzer, R., Sieger, R., Skjelvan, I., Sullivan, K. F., Sutherland, S. C., Sutton, A. J., Tadokoro, K., Telszewski, M., Tuma, M., Heuven, S. M. A. C. v., Vandemark, D., Ward, B., Watson, A. J., and Xu, S.: A multi-decade record of high-quality fCO$_2$ data in version 3 of the Surface Ocean CO$_2$ Atlas (SOCAT), Earth System Science Data, 8, 383–413, https://doi.org/https://doi.org/10.5194/essd-8-383-2016, https://www.earth-syst-sci-data.net/8/383/2016/, 2016.

Bauer, J. E., Cai, W.-J., Raymond, P. A., Bianchi, T. S., Hopkinson, C. S., and Regnier, P. A. G.: The changing carbon cycle of the coastal ocean, Nature, 504, 61–70, https://doi.org/10.1038/nature12857, https://www.nature.com/articles/nature12857, 2013.

Blanton, J. O.: Circulation processes along oceanic margins in relation to material fluxes, in: Ocean Margin Processes in Global Change, pp. 145–63, Wiley, New York, 1991.

Borges, A. V. and Gypens, N.: Carbonate chemistry in the coastal zone responds more strongly to eutrophication than ocean acidification, Limnology and Oceanography, 55, 346–353, https://doi.org/10.4319/lo.2010.55.1.0346, https://aslopubs.onlinelibrary.wiley.com/doi/abs/10.4319/lo.2010.55.1.0346, _eprint: https://aslopubs.onlinelibrary.wiley.com/doi/pdf/10.4319/lo.2010.55.1.0346, 2010.

Bourgeois, T., Orr, J. C., Resplandy, L., Terhaar, J., Ethé, C., Gehlen, M., and Bopp, L.: Coastal-ocean uptake of anthropogenic carbon, Biogeosciences, 13, 4167–4185, https://doi.org/https://doi.org/10.5194/bg-13-4167-2016, https://www.biogeosciences.net/13/4167/2016/, 2016.

Bricheno, L. M., Wolf, J. M., and Brown, J. M.: Impacts of high resolution model downscaling in coastal regions, Continental Shelf Research, 87, 7–16, https://doi.org/10.1016/j.csr.2013.11.007, http://www.sciencedirect.com/science/article/pii/S0278434313003725, 2014.

Cai, W.-J., Hu, X., Huang, W.-J., Murrell, M. C., Lehrter, J. C., Lohrenz, S. E., Chou, W.-C., Zhai, W., Hollibaugh, J. T., Wang, Y., Zhao, P., Guo, X., Gundersen, K., Dai, M., and Gong, G.-C.: Acidification of subsurface coastal waters enhanced by eutrophication, Nature Geosci, 4, 766–770, https://doi.org/10.1038/ngeo1297, https://www.nature.com/articles/ngeo1297, number: 11 Publisher: Nature Publishing Group, 2011.

Cavalieri, D. J., Parkinson, C. L., Gloersen, P., and Zwally, H. J.: Sea Ice Concentrations from Nimbus-7 SMMR and DMSP SSM/I-SSMIS Passive Microwave Data, Version 1, Monthly, doi:https://doi.org/10.5067/8GQ8LZQVL0VL, 1996.

Center, N. G. D.: 2-minute Gridded Global Relief Data (ETOPO2) v2, NOAA, https://doi.org/doi:10.7289/V5J1012Q, 2006.

"Cooperative Global Atmospheric Data Integration Project": Multi-laboratory compilation of atmospheric carbon dioxide data for the period 1968-2014, obspack_co2_1_GLOBALVIEWplus_v1.0_2015-07-30, https://doi.org/10.15138/G3RP42, published: NOAA Earth System Research Laboratory, Global Monitoring Division, 2015.

Couldrey, M. P., Oliver, K. I. C., Yool, A., Halloran, P. R., and Achterberg, E. P.: On which timescales do gas transfer velocities control North Atlantic CO2 flux variability?, Global Biogeochemical Cycles, 30, 787–802, https://doi.org/10.1002/2015GB005267, https://agupubs. onlinelibrary.wiley.com/doi/abs/10.1002/2015GB005267, 2016.

5 Desmit, X., Nohe, A., Borges, A. V., Prins, T., Cauwer, K. D., Lagring, R., Zande, D. V. d., and Sabbe, K.: Changes in chlorophyll concentration and phenology in the North Sea in relation to de-eutrophication and sea surface warming, Limnology and Oceanography, 65, 828–847, https://doi.org/10.1002/lno.11351, https://aslopubs.onlinelibrary.wiley.com/doi/abs/10.1002/lno.11351, _eprint: https://aslopubs.onlinelibrary.wiley.com/doi/pdf/10.1002/lno.11351, 2020.

Dickson, A. and Millero, F.: A comparison of the equilibrium constants for the dissociation of carbonic acid in seawater media, Deep-Sea Res. Pt I, 34, 1733 – 1743, https://doi.org/10.1016/0198-0149(87)90021-5, 1987.

10 Dickson, A. G.: Standard potential of the reaction: AgCl(s) + 12H2(g) = Ag(s) + HCl(aq), and and the standard acidity constant of the ion HSO4 in synthetic sea water from 273.15 to 318.15 K, The Journal of Chemical Thermodynamics, 22, 113–127, https://doi.org/10.1016/0021-9614(90)90074-Z, http://www.sciencedirect.com/science/article/pii/002196149090074Z, 1990.

Fay, A. R. and McKinley, G. A.: Correlations of surface ocean pCO2 to satellite chlorophyll on monthly to interannual timescales, Global Biogeochemical Cycles, 31, 436–455, https://doi.org/10.1002/2016GB005563, https://agupubs.onlinelibrary.wiley.com/doi/abs/10.1002/

15 2016GB005563, 2017.

Fröb, F., Olsen, A., Becker, M., Chafik, L., Johannessen, T., Reverdin, G., and Omar, A.: Wintertime fCO2 Variability in the Subpolar North Atlantic Since 2004, Geophysical Research Letters, 46, 1580–1590, https://doi.org/10.1029/2018GL080554, https://agupubs.onlinelibrary. wiley.com/doi/abs/10.1029/2018GL080554, 2019.

Gregg, W. W., Casey, N. W., and Rousseaux, C. S.: Sensitivity of simulated global ocean carbon flux estimates to forcing by reanalysis

20 products, Ocean Modelling, 80, 24–35, https://doi.org/10.1016/j.ocemod.2014.05.002, http://www.sciencedirect.com/science/article/pii/ S1463500314000651, 2014.

Griffiths, J. R., Kadin, M., Nascimento, F. J. A., Tamelander, T., Törnroos, A., Bonaglia, S., Bonsdorff, E., Brüchert, V., Gårdmark, A., Järnström, M., Kotta, J., Lindegren, M., Nordström, M. C., Norkko, A., Olsson, J., Weigel, B., Žydelis, R., Blenckner, T., Niiranen, S., and Winder, M.: The importance of benthic–pelagic coupling for marine ecosystem functioning in a changing world, Global Change Biology,

25 23, 2179–2196, https://doi.org/10.1111/gcb.13642, https://onlinelibrary.wiley.com/doi/abs/10.1111/gcb.13642, 2017.

Gruber, N., Clement, D., Carter, B. R., Feely, R. A., Heuven, S. v., Hoppema, M., Ishii, M., Key, R. M., Kozyr, A., Lauvset, S. K., Monaco, C. L., Mathis, J. T., Murata, A., Olsen, A., Perez, F. F., Sabine, C. L., Tanhua, T., and Wanninkhof, R.: The oceanic sink for anthropogenic CO2 from 1994 to 2007, Science, 363, 1193–1199, https://doi.org/10.1126/science.aau5153, http://science.sciencemag.org/content/363/ 6432/1193, 2019.

30 Ho, D. T. and Wanninkhof, R.: Air–sea gas exchange in the North Atlantic: 3He/SF6 experiment during GasEx-98, Tellus B: Chemical and Physical Meteorology, 68, 30 198, https://doi.org/10.3402/tellusb.v68.30198, https://doi.org/10.3402/tellusb.v68.30198, 2016.

Jones, S. D., Quéré, C. L., Rödenbeck, C., Manning, A. C., and Olsen, A.: A statistical gap-filling method to interpolate global monthly sur- face ocean carbon dioxide data, Journal of Advances in Modeling Earth Systems, 7, 1554–1575, https://doi.org/10.1002/2014MS000416, https://agupubs.onlinelibrary.wiley.com/doi/abs/10.1002/2014MS000416, 2015.

35 Kanamitsu, M., Ebisuzaki, W., Woollen, J., Yang, S.-K., Hnilo, J. J., Fiorino, M., and Potter, G. L.: NCEP–DOE AMIP-II Reanalysis (R-2), Bull. Amer. Meteor. Soc., 83, 1631–1644, https://doi.org/10.1175/BAMS-83-11-1631, https://journals.ametsoc.org/doi/abs/10.1175/ BAMS-83-11-1631, 2002.

Landschützer, P., Gruber, N., Bakker, D. C. E., Schuster, U., Nakaoka, S., Payne, M. R., Sasse, T. P., and Zeng, J.: A neural network-based estimate of the seasonal to inter-annual variability of the Atlantic Ocean carbon sink, Biogeosciences, 10, 7793–7815, https://doi.org/10.5194/bg-10-7793-2013, 2013.

Landschützer, P., Gruber, N., Bakker, D. C. E., and Schuster, U.: Recent variability of the global ocean carbon sink, Global Biogeochem. Cycles, 28, 927–949, https://doi.org/10.1002/2014GB004853, 2014.

Landschützer, P., Gruber, N., and Bakker, D. C. E.: Decadal variations and trends of the global ocean carbon sink, Global Biogeochemical Cycles, 30, 1396–1417, https://doi.org/10.1002/2015GB005359, https://agupubs.onlinelibrary.wiley.com/doi/abs/10.1002/2015GB005359, 2016.

Landschützer, P., Gruber, N., and Bakker, D. C. E.: An updated observation-based global monthly gridded sea surface pCO2 and air-sea CO2 flux product from 1982 through 2015 and its monthly climatology (NCEI Accession 0160558). Version 2.2., 2017.

Landschützer, P., Gruber, N., Bakker, D. C. E., Stemmler, I., and Six, K. D.: Strengthening seasonal marine CO 2 variations due to increasing atmospheric CO 2, Nature Climate Change, 8, 146, https://doi.org/10.1038/s41558-017-0057-x, https://www.nature.com/articles/s41558-017-0057-x, 2018.

Landschützer, P., Ilyina, T., and Lovenduski, N. S.: Detecting Regional Modes of Variability in Observation-Based Surface Ocean pCO2, Geophysical Research Letters, 0, https://doi.org/10.1029/2018GL081756, https://agupubs.onlinelibrary.wiley.com/doi/abs/10.1029/2018GL081756, 2019.

Laruelle, G. G., Dürr, H. H., Slomp, C. P., and Borges, A. V.: Evaluation of sinks and sources of CO2 in the global coastal ocean using a spatially-explicit typology of estuaries and continental shelves, Geophysical Research Letters, 37, https://doi.org/10.1029/2010GL043691, https://agupubs.onlinelibrary.wiley.com/doi/abs/10.1029/2010GL043691, 2010.

Laruelle, G. G., Dürr, H. H., Lauerwald, R., Hartmann, J., Slomp, C. P., Goossens, N., and Regnier, P. a. G.: Global multi-scale segmentation of continental and coastal waters from the watersheds to the continental margins, Hydrology and Earth System Sciences, 17, 2029–2051, https://doi.org/https://doi.org/10.5194/hess-17-2029-2013, https://www.hydrol-earth-syst-sci.net/17/2029/2013/, 2013.

Laruelle, G. G., Landschützer, P., Gruber, N., Tison, J.-L., Delille, B., and Regnier, P.: Global high-resolution monthly pCO$_2$ climatology for the coastal ocean derived from neural network interpolation, Biogeosciences, 14, 4545–4561, https://doi.org/https://doi.org/10.5194/bg-14-4545-2017, https://www.biogeosciences.net/14/4545/2017/, 2017.

Laruelle, G. G., Cai, W.-J., Hu, X., Gruber, N., Mackenzie, F. T., and Regnier, P.: Continental shelves as a variable but increasing global sink for atmospheric carbon dioxide, Nature Communications, 9, 454, https://doi.org/10.1038/s41467-017-02738-z, https://www.nature.com/articles/s41467-017-02738-z, 2018.

Lauvset, S. K. and Gruber, N.: Long-term trends in surface ocean pH in the North Atlantic, Marine Chemistry, 162, 71–76, https://doi.org/10.1016/j.marchem.2014.03.009, https://www.sciencedirect.com/science/article/pii/S0304420314000607, 2014.

Lauvset, S. K., Gruber, N., Landschützer, P., Olsen, A., and Tjiputra, J.: Trends and drivers in global surface ocean pH over the past 3 decades, Biogeosciences, 12, 1285–1298, https://doi.org/https://doi.org/10.5194/bg-12-1285-2015, https://www.biogeosciences.net/12/1285/2015/, 2015.

Lima, F. P. and Wethey, D. S.: Three decades of high-resolution coastal sea surface temperatures reveal more than warming, Nat Commun, 3, 1–13, https://doi.org/10.1038/ncomms1713, https://www.nature.com/articles/ncomms1713, 2012.

Lind, S., Ingvaldsen, R. B., and Furevik, T.: Arctic warming hotspot in the northern Barents Sea linked to declining sea-ice import, Nature Clim Change, 8, 634–639, https://doi.org/10.1038/s41558-018-0205-y, https://www.nature.com/articles/s41558-018-0205-y, 2018.

Locarnini, R., Mishonov, A., Baranova, O., Boyer, T., Zweng, M., GarciA, H., Reagan, J., Seidov, D., Weathers, K., Paver, C., and Smoylar, I.: World Ocean Atlas 2018, Volume 1: Temperature, A. Mishonov Technical Ed., 2018.

Loose, B., McGillis, W. R., Schlosser, P., Perovich, D., and Takahashi, T.: Effects of freezing, growth, and ice cover on gas transport processes in laboratory seawater experiments, Geophysical Research Letters, 36, https://doi.org/10.1029/2008GL036318, https://agupubs.
onlinelibrary.wiley.com/doi/abs/10.1029/2008GL036318, 2009.

Mehrbach, C., Culberson, C., Hawley, J., and Pytkowicz, R.: Measurement of the apparent dissociation constants of carbonic acid in seawater at atmospheric pressure, Limnol. Oceanogr., 18, 897–907, 1973.

Meyer, M., Pätsch, J., Geyer, B., and Thomas, H.: Revisiting the Estimate of the North Sea Air-Sea Flux of CO2 in 2001/2002: The Dominant Role of Different Wind Data Products, Journal of Geophysical Research: Biogeosciences, 123, 1511–1525, https://doi.org/10.1029/2017JG004281, https://agupubs.onlinelibrary.wiley.com/doi/abs/10.1029/2017JG004281, 2018.

Müller, J. D., Schneider, B., and Rehder, G.: Long-term alkalinity trends in the Baltic Sea and their implications for CO2-induced acidification, Limnology and Oceanography, 61, 1984–2002, https://doi.org/10.1002/lno.10349, https://aslopubs.onlinelibrary.wiley.com/doi/abs/10.1002/lno.10349, 2016.

Naegler, T.: Reconciliation of excess 14C-constrained global CO2 piston velocity estimates, Tellus B: Chemical and Physical Meteorology, 61, 372–384, https://doi.org/10.1111/j.1600-0889.2008.00408.x, https://doi.org/10.1111/j.1600-0889.2008.00408.x, 2009.

Nondal, G., Bellerby, R. G. J., Oldenc, A., Johannessena, T., and Olafssond, J.: Optimal evaluation of the surface ocean CO2 system in the northern North Atlantic using data from voluntary observing ships, Limnol. Oceanogr., 7, 109–118, 2009.

Omar, A. M., Olsen, A., Johannessen, T., Hoppema, M., Thomas, H., and Borges, A. V.: Spatiotemporal variations of f CO2 in the North Sea, Ocean Sci., p. 13, 2010.

Omar, A. M., Thomas, H., Olsen, A., Becker, M., Skjelvan, I., and Reverdin, G.: Trend of ocean acidification and pCO2 in the northern North Sea, 2004-2015, Journal of Geophysical Research - Biogeosciences, 2019.

Oziel, L., Neukermans, G., Ardyna, M., Lancelot, C., Tison, J.-L., Wassmann, P., Sirven, J., Ruiz-Pino, D., and Gascard, J.-C.: Role for Atlantic inflows and sea ice loss on shifting phytoplankton blooms in the Barents Sea, Journal of Geophysical Research: Oceans, pp. 5121–5139, https://doi.org/10.1002/2016JC012582@10.1002/(ISSN)2169-9291.ARCTICJOINT, https://agupubs.onlinelibrary.wiley.com/doi/abs/10.1002/2016JC012582%4010.1002/%28ISSN%292169-9291.ARCTICJOINT, 2016.

Parard, G., Charantonis, A. A., and Rutgersson, A.: Using satellite data to estimate partial pressure of CO $_2$ in the Baltic Sea: PARTIAL PRESSURE OF CO $_2$ VARIABILITY, Journal of Geophysical Research: Biogeosciences, 121, 1002–1015, https://doi.org/10.1002/2015JG003064, http://doi.wiley.com/10.1002/2015JG003064, 2016.

Parard, G., Rutgersson, A., Raj Parampil, S., and Charantonis, A. A.: The potential of using remote sensing data to estimate air–sea CO₂ exchange in the Baltic Sea, Earth System Dynamics, 8, 1093–1106, https://doi.org/10.5194/esd-8-1093-2017, https://www.earth-syst-dynam.net/8/1093/2017/, 2017.

Pierrot, D., Neill, C., Sullivan, K., Castle, R., Wanninkhof, R., Lüger, H., Johannessen, T., Olsen, A., Feely, R. A., and Cosca, C. E.: Recommendations for autonomous underway $p\mathrm{CO_2}$ measuring systems and data-reduction routines, Surface Ocean CO2 Variability and Vulnerabilities, 56, 512–522, https://doi.org/10.1016/j.dsr2.2008.12.005, 2009.

Roobaert, A., Laruelle, G. G., Landschützer, P., and Regnier, P.: Uncertainty in the global oceanic CO$_2$ uptake induced by wind forcing: quantification and spatial analysis, Biogeosciences, 15, 1701–1720, https://doi.org/https://doi.org/10.5194/bg-15-1701-2018, https://www.biogeosciences.net/15/1701/2018/, 2018.

Rödenbeck, C., Keeling, R. F., Bakker, D. C. E., Metzl, N., Olsen, A., Sabine, C., and Heimann, M.: Global surface-ocean pCO2 and sea–air CO2 flux variability from an observation-driven ocean mixed-layer scheme, Ocean Sci., 9, 193–216, https://doi.org/10.5194/os-9-193-2013, https://www.ocean-sci.net/9/193/2013/, 2013.

Rödenbeck, C., Bakker, D. C. E., Metzl, N., Olsen, A., Sabine, C., Cassar, N., Reum, F., Keeling, R. F., and Heimann, M.: Interannual sea–air CO_2 flux variability from an observation-driven ocean mixed-layer scheme, Biogeosciences, 11, 4599–4613, https://doi.org/https://doi.org/10.5194/bg-11-4599-2014, https://www.biogeosciences.net/11/4599/2014/bg-11-4599-2014.html, 2014.

Rödenbeck, C., Bakker, D. C. E., Gruber, N., Iida, Y., Jacobson, A. R., Jones, S., Landschützer, P., Metzl, N., Nakaoka, S., Olsen, A., Park, G.-H., Peylin, P., Rodgers, K. B., Sasse, T. P., Schuster, U., Shutler, J. D., Valsala, V., Wanninkhof, R., and Zeng, J.: Data-based estimates of the ocean carbon sink variability – first results of the Surface Ocean pCO$_2$ Mapping intercomparison (SOCOM), Biogeosciences, 12, 7251–7278, https://doi.org/https://doi.org/10.5194/bg-12-7251-2015, https://www.biogeosciences.net/12/7251/2015/, 2015.

Salt, L. A., Thomas, H., Prowe, A. E. F., Borges, A. V., Bozec, Y., and Baar, H. J. W. d.: Variability of North Sea pH and CO2 in response to North Atlantic Oscillation forcing, Journal of Geophysical Research: Biogeosciences, 118, 1584–1592, https://doi.org/10.1002/2013JG002306, https://agupubs.onlinelibrary.wiley.com/doi/abs/10.1002/2013JG002306, 2013.

Schiettecatte, L. S., Thomas, H., Bozec, Y., and Borges, A. V.: High temporal coverage of carbon dioxide measurements in the Southern Bight of the North Sea, Marine Chemistry, 106, 161–173, https://doi.org/10.1016/j.marchem.2007.01.001, http://www.sciencedirect.com/science/article/pii/S0304420307000023, 2007.

Schneider, B. and Müller, J. D.: Biogeochemical Transformations in the Baltic Sea: Observations Through Carbon Dioxide Glasses, Springer Oceanography, Springer International Publishing, https://www.springer.com/gp/book/9783319616988, 2018.

Sharples, J., Ross, O. N., Scott, B. E., Greenstreet, S. P. R., and Fraser, H.: Inter-annual variability in the timing of stratification and the spring bloom in the North-western North Sea, Cont.Shelf Res., 26, 733–751, https://doi.org/10.1016/j.csr.2006.01.011, https://abdn.pure.elsevier.com/en/publications/inter-annual-variability-in-the-timing-of-stratification-and-the-, 2006.

Thomas, H., Bozec, Y., Elkalay, K., and Baar, H. J. W. d.: Enhanced Open Ocean Storage of CO2 from Shelf Sea Pumping, Science, 304, 1005–1008, https://doi.org/10.1126/science.1095491, https://science.sciencemag.org/content/304/5673/1005, 2004.

Thomas, H., Friederike Prowe, A. E., van Heuven, S., Bozec, Y., de Baar, H. J. W., Schiettecatte, L.-S., Suykens, K., Koné, M., Borges, A. V., Lima, I. D., and Doney, S. C.: Rapid decline of the CO2 buffering capacity in the North Sea and implications for the North Atlantic Ocean, Global Biogeochemical Cycles, 21, https://doi.org/10.1029/2006GB002825, https://agupubs.onlinelibrary.wiley.com/doi/full/10.1029/2006GB002825, 2007.

Uppström, L. R.: The boron/chlorinity ratio of deep-sea water from the Pacific Ocean, Deep Sea Research and Oceanographic Abstracts, 21, 161–162, https://doi.org/10.1016/0011-7471(74)90074-6, http://www.sciencedirect.com/science/article/pii/0011747174900746, 1974.

van Heuven, S., Pierrot, D., Lewis, E., and Wallace, D.: {MATLAB} Program Developed for {CO}$_2$ System Calculations. {ORNL/CDIAC}-105b., 2009.

Wanninkhof, R.: Relationship between wind speed and gas exchange over the ocean revisited: Gas exchange and wind speed over the ocean, Limnology and Oceanography: Methods, 12, 351–362, https://doi.org/10.4319/lom.2014.12.351, http://doi.wiley.com/10.4319/lom.2014.12.351, 2014.

Weiss, R. F.: Carbon dioxide in water and seawater: The solubility of a non-ideal gas, Mar. Chem., 2, 203–215, 1974.

Wesslander, K., Omstedt, A., and Schneider, B.: Inter-annual and seasonal variations in the air–sea CO2 balance in the central Baltic Sea and the Kattegat, Continental Shelf Research, 30, 1511–1521, http://www.academia.edu/16389763/Inter-annual_and_seasonal_variations_in_the_air_sea_CO2_balance_in_the_central_Baltic_Sea_and_the_Kattegat, 2010.

Wollast, R.: Evaluation and comparison of the global carbon cycle in the coastal zone and in the open ocean, in: The Sea, edited by Brink, K. H. and Robinson, A. R., pp. 213–252, John Wiley & Sons, New York, 1998.

Yasunaka, S., Siswanto, E., Olsen, A., Hoppema, M., Watanabe, E., Fransson, A., Chierici, M., Murata, A., Lauvset, S. K., Wanninkhof, R., Takahashi, T., Kosugi, N., Omar, A. M., Heuven, S. v., and Mathis, J. T.: Arctic Ocean CO_2 uptake: an improved multiyear estimate of the air–sea CO_2 flux incorporating chlorophyll a concentrations, Biogeosciences, 15, 1643–1661, https://doi.org/https://doi.org/10.5194/bg-15-1643-2018, https://www.biogeosciences.net/15/1643/2018/, 2018.